UNIVERSIDADE D
COIMBRA

PRINCESS STEPHANIE LLANOS

Characterization of industrial made TiAlN, TiAlCN and TiAlN/TiAlCN coatings used for machining of Ti6Al4V aerospace alloy

VOLUME 1

Dissertação no âmbito do Mestrado Conjunto Europeu em Tribologia de Superfícies e Interfaces orientada pelos Doutor Filipe Daniel Fernandes and Doutor Abbas Al-Rjoub e apresentada ao Departamento de Engenharia Mecânica da Faculdade de Ciências e Tecnologia da Universidade de Coimbra.

Julho de 2021

1 2 9 0

FACULDADE DE CIÊNCIAS E TECNOLOGIA
UNIVERSIDADE D COIMBRA

Characterization of industrial made TiAlN, TiAlCN and TiAlN/TiAlCN coatings used for machining of Ti6Al4V aerospace alloy

Submitted in Partial Fulfilment of the Requirements for the Degree of European Joint European Master in Tribology of Surfaces and Interfaces.

Caracterização de revestimentos industriais do tipo TiAlN, TiAlN e TiAlN/TiAlN usados para maquinação da liga Ti6Al4V usada em aplicações aeronáuticas

Author

Princess Stephanie Llanos

Advisors

Dr. Filipe Daniel Fernandes

Dr. Abbas Al-Rjoub

Jury

President	**Professor Bruno Miguel Quelhas de Sacadura Cabral Trindade** **Professor at University of Coimbra**
Vowel	**Professor Amílcar Lopes Ramalho** **Professor at University of Coimbra**
Advisor	**Doctor Filipe Daniel Fernandes** **Invited Assistant Professor at University of Coimbra**

---

1 2 9 0

UNIVERSIDADE D COIMBRA

tribos

Joint European Master in Tribology of Surfaces and Interfaces

Ljubljana • Leeds • Coimbra • Luleå

Coimbra, Julho de 2021

ACKNOWLEDGEMENTS

I would like to express my sincere gratitude and appreciation to the following who contributed in one way or another to the completion of this thesis project:

First of all, thanks to my supervisor, Dr. Filipe Daniel Fernandes, for his guidance and patience throughout the duration of the study. His expertise and knowledge in the field, which greatly helped me from the conceptualization of the project to the analysis of results and writing of the manuscript, are much appreciated. I would also like to thank the jury members, Professor Bruno Trindade and Professor Amílcar Ramalho for their valuable inputs during the thesis presentation.

Thank you to Dr. Abbas Al-Rjoub for being directly involved in my project by guiding me throughout the experimentation process. He has supported me in performing and arranging the equipment needed for the different characterization techniques involved in the project. My appreciation also extends to Dr. Talha Yaqub and Dr. Carlos Patacas for their assistance during the tribological tests and SEM-EDS characterization, respectively.

Huge thanks to the Joint European Master of Tribology of Surfaces and Interfaces program and the coordinators for this opportunity and their support during the entire duration of the program. This study was also sponsored by FEDER funds through the COMPETE program and under the project MCTool21 – POCI-01-0247-FEDER-045940.

To my TRIBOS batchmates (both in Portugal and in Sweden), the people whom I relate to with the ups and downs of performing the thesis, thank you for the energy, laughter and meaningful discussions.

I would also like to thank my family and friends back home for supporting me despite the distance. And lastly, thank you to Ino Rupisan for always pushing me to do my best and cheering me on.

Abstract

The research and development on titanium alloys have been nourishing for quite some time due to their superior physical, chemical and mechanical properties. However, manufacturing titanium is more expensive and requires longer time compared with other metals due to its poor machinability. One of the leading solutions to address the difficulty in machining titanium is to deposit coating on the cutting tools in order lengthen the service lifetime and ensure good quality of machined surface. In this study, industrial made monolithic TiAlN, monolithic TiAlCN and multilayered TiAlN/TiAlCN coatings were thoroughly characterized to determine which coating displayed the best combination of properties. The deposited coatings were fully characterized for their chemical composition, structure and morphology, oxidation resistance, thermal stability, mechanical properties and tribological performance at room temperature. The coatings reported different chemical composition of Ti, Al, N and C due to the different targets, chemical composition and power applied to the target during deposition. All films displayed a fcc NaCl type structure. The SEM micrographs of the cross-section and surface morphology of the as-deposited coatings exhibited a columnar growth with TiAlN showing the densest structure. The onset point of oxidation was measured to be ~900°C, ~850°C and ~800°C for TiAlN, TiAlCN and TiAlN/TiAlCN, respectively. After the isothermal test at 900°C for 2 h, TiAlCN and TiAlN/TiAlCN were fully oxidized while a huge portion of the TiAlN coating still exists. The remarkable oxidation resistance of the latter coating was driven by the formation of a continuous and protective oxide scale Al_2O_3 on top of the oxide layer. The presence of this

oxide scale was confirmed by XRD, SEM micrograph and elemental map distribution. The as-deposited TiAlN/TiAlCN reported the highest H and E values at 38 GPa and 374 GPa, respectively. Upon annealing, TiAlN exhibited an increase in hardness due to increase in crystallinity. In the tribological tests, the coefficient of friction, wear depth and wear rate corroborate the hardness and toughness results of the coatings. The wear track exhibit abrasion mechanism which is characterized by grooves and scratches and the presence of wear debris. The multilayered TiAlN/TiAlCN showed the best tribological performance due to the combination of high hardness and high fracture toughness compared to the monolithic TiAlN and TiAlCN coatings.

Keywords Titanium alloy, TiAlN, TiAlCN, Oxidation resistance, Thermal stability, Tribological performance.

Resumo

A investigação e desenvolvimento de ligas de titânio tem vindo a ser alvo de estudo durante as últimas décadas devido às suas superiors propriedades físicas, químicas e mecânicas quando comparado com outros ligas. No entanto, o fabrico de components em ligas de titânio é mais caro e requer mais tempo de processamento em comparação com outros metais devido à sua grande dificuldade de maquinar. Uma das principais soluções atualmente usadas para melhorar a maquinação das ligas de titânio é a aplicação de revestimentos na superficie das ferramentas de corte, que por um lado permitem aumentar a vida de ferramenta de corte e por outro melhorar a qualidade da superfície maquinada.

Nesta tese, revestimentos industriais depositados em monocamada (TiAlN, TiAlCN) e em multicamada (TiAlN/TiAlCN) foram caracterizados relativamente a diferentes propriedades para determiner quais dos revestimentoa apresentam o melhor compromisso entre propriedades. Os revestimentos depositados foram caracterizados quanto à sua composição química, estrutura, morfologia, resistência à oxidação, estabilidade térmica, propriedades mecânicas e comportamento tribológico à temperatura ambiente. Como esperado os revestimentos apresentam diferentes composições químicas de Ti, Al, N e C devido à diferente composição dos alvos usados e potência aplicadas aos alvos durante a deposição. Todos os revestimentos apresentam uma estrutura fcc. A morfologia dos revestimentos em secção transversal exibem um crescimento columnar, onde o revestimento TiAlN apresenta uma morfologia mas densa do ques os outros revestimentos. O ponto de início de oxidação dos revestimentos é dependente da composição química dos revestimentos: ~900°C, ~850°C e ~800°C para os revestimentos TiAlN, TiAlCN e

TiAlN/TiAlCN, respectivamente. Os testes isotérmicos realizados às amostras a 900°C durante 2 h aos revestimentos, promoveram a total oxidação dis revestimentos TiAlCN e TiAlN/TiAlCN, enquanto que o revestimento TiAlN foi apenas parcialmente oxidado. A notável resistência à oxidação do revestimento TiAlN deve-se à formação de uma camada continua e protetora de Al_2O_3 no topo da camada de óxido. A formação dessa fase foi identificada por difração de raios-x analyses SEM. O revestimento TiAlN/TiAlCN apresentou os maiores valores de dureza – 38 GPa e modulo de elastecidade – 374 GPa, entre os diferentes revestimentos. Após o recozimento, o revestimento TiAlN exibiu um aumento de dureza devido ao aumento da sua cristalinidade. Nos testes tribológicos, o coeficiente de atrito, a profundidade de desgaste e a taxa especifica de desgaste corroboram os resultados de dureza e tenacidade. As pistas de desgaste exibem um mecanismo de abrasão, caracterizadas pela presença de ranhuras e detritos. O revestiemnto TiAlN/TiAlCN apresentou o melhor desempenho tribológico devido à combinação de alta dureza e alta tenacidade à fratura em comparação coms outros revestimentos.

Palavra-chave Ligas de titânio, Revestimentos dos sistemas TiAlN e TiAlCN, Resistência à oxidação, Estabilidade térmica, Desempenho tribológico.

TABLE OF CONTENTS

LIST OF FIGURES

LIST OF TABLES

CHAPTER 1: INTRODUCTION

1.1 Motivation

The growing interest on research and development of titanium and its alloys for a wide range of applications stems from its superior physical, mechanical and chemical properties. Titanium alloys have a high strength-to-weight ratio, exceptional corrosion resistance, low thermal expansion and excellent biocompatibility [1-2]. The low density combined with high strength and fracture toughness properties allow the use of titanium alloys in applications that require reduction in weight while the low thermal expansion allows operation at high temperature [2]. The exceptional resistance to corrosion is driven by its ability to passivate and form a stable oxide layer, in the form of TiO_2, which acts as a protective film to shield the surface [3]. Furthermore, titanium is non-toxic and is generally compatible with human tissues and bones. Due to these material properties, titanium alloys are classified as superalloys [4].

The application of titanium and its alloys has considerably grown in numerous industries over the past few decades. The combination of high strength-to-weight ratio and good corrosion resistance makes titanium a promising material for aeronautic and aerospace applications, where about 80% of titanium alloys produced are utilized [5]. The ability of titanium to withstand aggressive environments makes it the material of choice in various industrial applications such as pulp and paper manufacture, oil production and piping systems. Current medical and dental procedures involve the use of titanium in implants, external prostheses and instruments which depend on the high strength, low density and biocompatibility of titanium. The use of titanium alloys has also penetrated the consumer industry in the form of jewelry, sports equipment and automotive applications [5-6]. As a result of these specialized applications, titanium and its alloys are normally processed under rigorous conditions. Despite the high demand and production, the cost of manufacturing titanium is more expensive and requires longer manufacturing time compared to other metals mainly due to its poor machinability [1-2].

Machining difficult-to-machine materials such as titanium and its alloys can often lead to reduced lifetime of cutting tool and poor surface finish quality of the workpiece [7-8]. Over the past few decades, several solutions have been developed to address the poor machinability of titanium alloys which include low speed machining, thermally assisted machining, use of liquid coolant during operation, application of coatings and the combination of one or more of these methods. One of the most utilized, among the available solutions, is the use of hard coating on the surface of cutting tools [4,9-10].

Hard metal coatings have been widely used to extend cutting tool lifetime and overall tool performance when cutting difficult-to-machine materials such as titanium and its alloys. Coatings offer better mechanical, thermal and tribological properties for the tools such as higher surface hardness, better oxidation resistance, thermal stability and reduced friction coefficient during machining operation. The use of coated tools can reduce cutting forces and enable higher machining speed without compromising tool life and machined surface quality [10-12]. Additionally, the use of coating permits dry machining operations which is considered as a promising way to achieve the goals of sustainable machining while keeping the machining cost to minimum [11].

Among the currently available hard coatings for cutting tools, titanium aluminum nitride (TiAlN) based coatings are commonly used for machining applications [10]. Aside from the enhanced mechanical properties, TiAlN-based coatings can offer improved oxidation resistance and enhanced tribological performance compared with other coatings which are essential for dry machining conditions [13-16]. However, there is limited information on the systematic characterization and comparison between the different properties of TiAlN-based coatings, especially for coatings developed in an industrial scale which is relevant to machining operations. Thus, a systematic evaluation and comparison of the different properties of these types of coatings would be beneficial. This thesis is focused on the characterization and comparison of the chemical composition, mechanical, thermal and tribological properties of industrial supplied (name of supplier redacted due to confidentiality matters) coatings used to protect the surface of cutting tools used for machining titanium alloys.

1.2 Objectives of the Study

It has been reported by numerous studies on coatings that TiAlN has a superior oxidation resistance which makes it an effective coating system for machining operations at elevated temperatures [13-14,17]. Additionally, the incorporation of C atoms to TiAlN coating can help lower the friction coefficient between surface contacts during machining [15-16,18]. These coating systems help prolong the cutting tool service lifetime when dry machining titanium and its alloys. With these knowledge, three industrial coating systems, namely monolithic TiAlN and TiAlCN and multilayered TiAlN/TiAlCN, have been thoroughly characterized in this thesis regarding their chemical composition, mechanical, thermal and tribological properties.

The aim is to determine and verify which of the industrial coatings displayed the best compromise of properties. Consequently, the coating which can best protect the surface of cutting tools is identified. The main objective of the study was accomplished by fulfilling the following sub-objectives:

i. Deposition of industrial monolithic TiAlN and TiAlCN and multilayered TiAlN/TiAlCN coatings by sputtering at an enterprise premises, using DC power supplies and different targets.

ii. Investigate the structure, chemical composition and morphology of the coatings.

iii. Investigate the mechanical properties of the coatings.

iv. Analyze the oxidation resistance and thermal stability of the coatings.

v. Evaluate the tribological performance using pin-on-disk test at room temperature.

vi. Compare the properties and select the industrial coating with the best performance.

CHAPTER 2: STATE OF ART

2.1 Machinability of Titanium Alloys

Machining is one of the most accurate manufacturing processes for producing components of different geometric features [2]. It involves the removal of material using a cutting tool to achieve a desired final shape, size and surface finish [19]. Figure 2.1 shows a conventional machining operation wherein a surface layer is removed, in the form of chips, by the relative movement between a sharp cutting tool and workpiece. The chip formation mechanism is governed by shear deformation wherein the material is assumed to shear along a shear plane which extends from the tool tip to the surface [7].

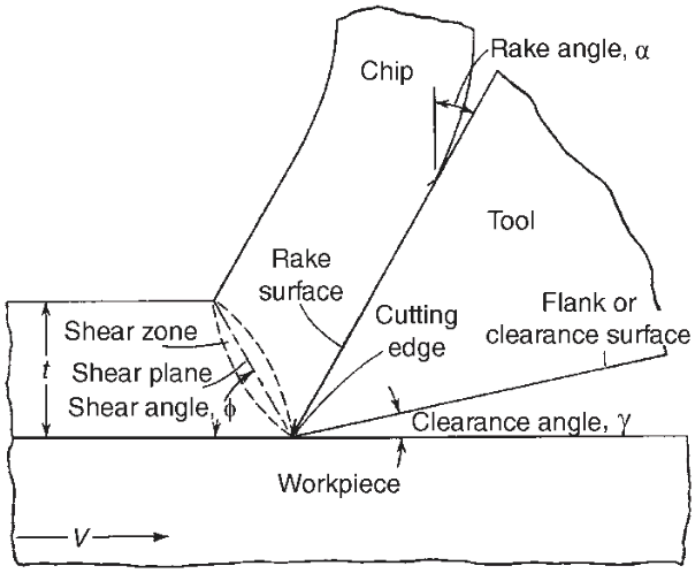

Figure 2.1 Schematic diagram of the cutting zone during turning operations.

Machining is usually characterized with excessive heat generation at the cutting zone which strongly influences the wear rate, lifetime of cutting tool and workpiece surface integrity. Due to its poor machinability, machining of titanium alloys usually entails higher operational cost and lower productivity [2]. The poor machinability of titanium alloys is due to several inherent material characteristics which subject cutting tool materials to severe thermal and mechanical stresses, often leading to plastic deformation and significant reduction in tool lifetime [1].

Titanium and its alloys are considered as difficult-to-machine materials due to poor thermal conductivity, low modulus of elasticity and high chemical reactivity [2-4]. During machining, there is an excessive generation of heat at the tool-workpiece interface which results in high cutting temperature. Due to the low thermal conductivity of titanium, majority of the heat generated flows to the cutting edge of the tool instead of being dissipated into the chip. The thermal stress experienced by the tool cutting edge results to increase in tool wear. Additionally, since titanium maintains its high strength at elevated temperature, higher machining force is required despite the cutting tool suffering from heat softening. The low modulus of elasticity results to workpiece chatter and deflection causing uneven machined surface. Lastly, titanium is a highly reactive material; thus, it tends to weld to the cutting tool material during machining which may lead to adhesion and diffusion wear [2].

The machinability problem limits the tool life of any cutting tool used to cut titanium alloys during the manufacturing process. This hinders the continuous market growth of titanium alloys as the cost of production skyrockets when machining cost is involved. One major motivation of research studies on titanium in the past few decades is to reduce the cost of manufacturing. To achieve this goal and address the machinability issues, research studies have focused on: (1) the enhancement of cutting tool efficiency, (2) development of new bulk materials which are harder and with higher thermal conductivity, (3) development of new coating systems to protect the cutting tools, (4) identification of optimal combination of tool and cutting parameters and (5) expansion of advanced hybrid machining processes [7]. Extensive investigation on machining processes, cutting tool materials and machining techniques is needed to address the inferior machinability of titanium and its alloys.

2.2 Types of Machining Processes

Machining includes several processes that is used to transform casting, forging or any other preformed block of materials into the final desired product. The operations that allow machining of titanium alloys include turning, milling, drilling, reaming, tapping, sawing and grinding [20]. A recent review by Rizzo et al. [21] on cutting tools for machining identified turning, drilling and milling as the mostly used machining operations, capturing almost 87% of the total tooling market as shown in Figure 2.2. Unlike other methods that require the assistance of cutting fluid, these processes successfully adapted to dry machining [19].

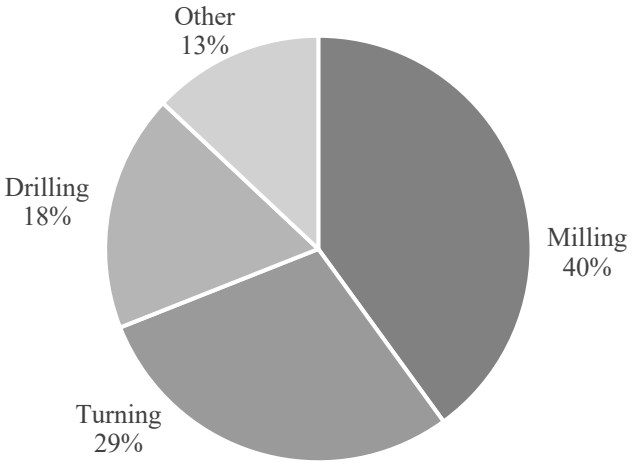

Figure 2.2 Cutting Technology Global Market Distribution.

Turning involves the removal of material from a rotating cylindrical workpiece using a cutting tool that moves in a linear motion to form a profile. The workpiece is held by the lathe chuck and rotated at a pre-determined speed while the tool is held rigidly in a tool holder and moved at a constant rate along the axis of the workpiece. A schematic diagram of a turning operation is shown in Figure 2.3 [7].

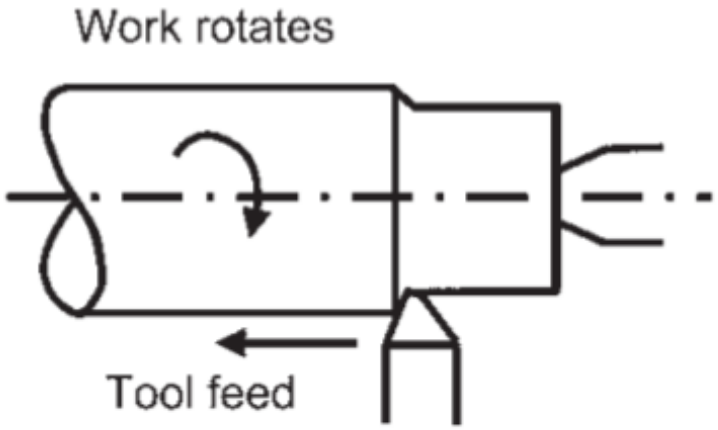

Figure 2.3 Machining operation: Turning.

Drilling is a material-removing process wherein a cutting tool, referred to as a drill bit, cuts a hole in the workpiece. The drill bit is pressed against a stationary workpiece and rotated at rates up to thousands of revolutions per minute. The use of automatic drilling is preferred over hand drilling to reduce operator fatigue and ensure identical hole size. Figure 2.4 shows a schematic diagram of a typical drilling operation [7].

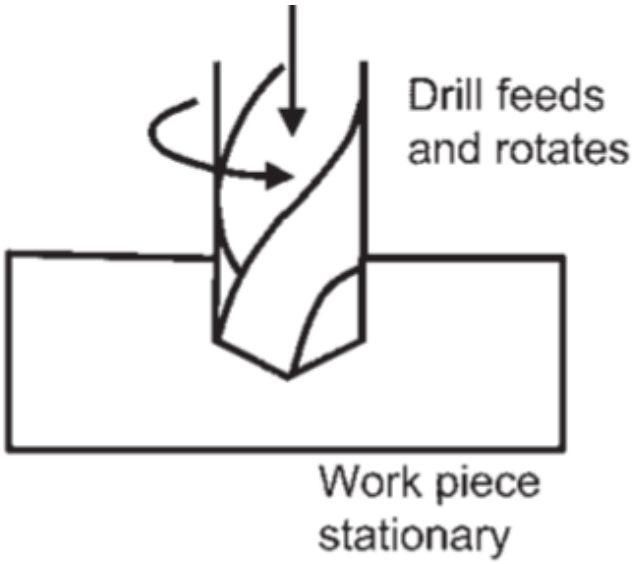

Figure 2.4 Machining operation: Drilling.

Milling is a machining technique in which a material is removed by the relative motion between the workpiece and a rotating multiple-tooth cutter. As illustrated in Figure 2.5, the contact between the cutting tool and workpiece is intermittent, with each tooth able to remove a small amount of workpiece with each revolution of the cutter. The machined parts are usually not axially symmetric and have many features, such as holes, pockets, grooves and even 3D surfaces [7].

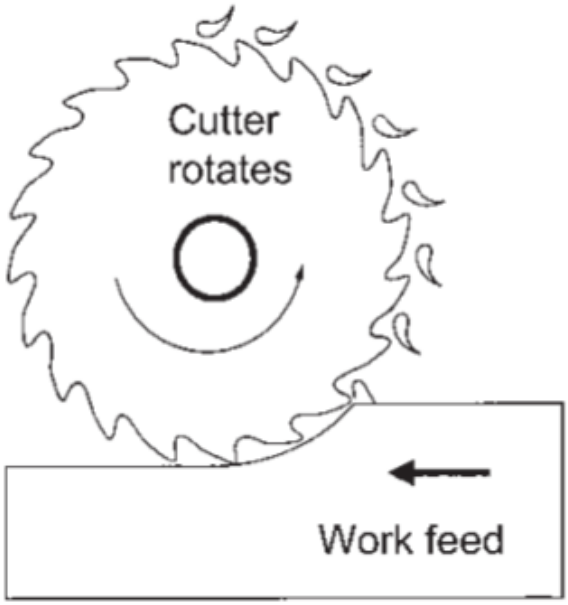

Figure 2.5 Machining operation: Milling.

2.3 Materials for Machining Tools

Selecting the appropriate cutting tool material for a certain machining process is crucial to ensure an effective machining operation. The relationship between the cutting tool and the workpiece to be machined significantly impact the total cost of the operation as it affects the cutting conditions and surface finish quality [22]. The study of Rizzo et al. [21] summarized the cutting tool materials that currently dominate the market which include cemented carbides, high-speed-steels, ceramics, super hard materials and cermets. The global market distribution of these materials according to this review is shown in Figure 2.6.

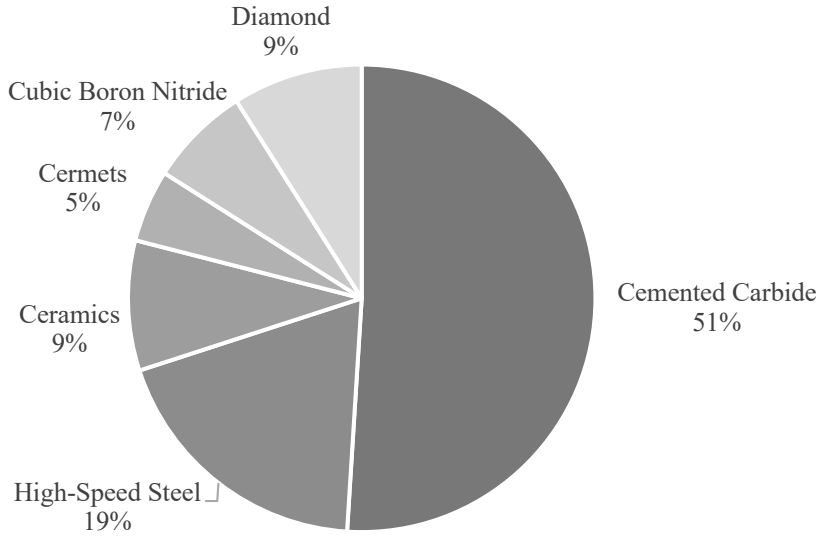

Figure 2.6 Cutting Tool Material Global Market Distribution.

Cemented carbide is the widely used cutting tool material with a distribution of 51%. This type of material shows relatively promising results when machining titanium alloys due to its high hardness and melting point. It is made up of hard carbides of group IVB – VIB metals bounded together by cobalt or nickel metal binder which offers high wear resistance and compressive strength, thereby allowing the cutting of material at high removal rates [7]. These rigid and strongly bonded compounds do not undergo any significant structural changes up to the melting temperature. Unlike steel which can be softened by annealing and hardened by rapid cooling, the properties of cemented carbide remain unaffected by the change in temperature which makes it a good material for cutting tools [21]. Table 2.1 shows a list of commonly used cemented carbide cutting tool materials with their corresponding hardness and melting temperatures [23].

Table 2.1
Cemented carbide tool properties.

Carbides	Melting Point (°C)	Hardness (HV)
WC	2,750	2,100
TiC	3,200	3,200
TbC	3,500	2,400
TaC	3,900	1,800

High-speed steel (HSS) can machine materials at higher cutting speeds through the retention of compressive strength at 550°C to 650°C [23]. With 19% global market distribution, the improved wear resistance and hot hardness of HSS are due to alloying to the base carbon steel, such as tungsten, molybdenum, chromium, vanadium or any combination of these elements. Above 650°C, HSS weaken and incur permanent structural changes which limit the metal removal rate of the cutting tool [7,23]. Ceramic tool materials, which comprise 9% of the global market distribution, can be alumina-based or silicon nitride-based. This type of cutting material can retain its hardness at elevated operating temperatures. However, it has poor fracture toughness which makes it susceptible to mechanical and thermal shock during machining. Generally, ceramic tools are not recommended for titanium alloys machining due to the increased wear rate driven by poor thermal conductivity, low fracture toughness and high reactivity with titanium alloys [1]. Cutting tool materials such as polycrystalline diamond (PCD) and cubic boron nitride (CBN) are effective due to their high hardness and extreme wear resistance. However, CBN and PCD are 10 to 20 times more expensive than tools based on cemented carbide. The high cost of these cutting tool materials would disregard the goal to reduce the machining cost of titanium alloys [1].

Despite the global market distribution, these materials are not entirely successful in improving the machinability of titanium alloys due to the demanding requirements needed to be met such as high hardness at elevated temperatures, excellent thermal conductivity, chemical inertness to avoid reaction with titanium, improved fatigue resistance and high compressive, tensile and shear strengths [22]. Knowing the limitations of the cutting tools that dominate the market, the challenge is to enhance the properties or find alternative materials to address the difficulty of machining titanium alloys.

2.4 Solutions to Improve Machinability

Understanding the failure mechanism and contributing factors associated with machining titanium alloy can help avoid or delay the cutting tool damage. This would result to reduced machining cost due to prolonged cutting tool life and increased operational productivity due to improved surface quality. Over the past few decades, several techniques have been developed to improve the machinability of titanium alloys which include the following:

a) Low speed machining: This technique allows machining operations to be performed at low cutting speed to help reduce tool edge temperature thereby prolonging tool life. However, machining at low speed is neither economical nor practical as it results to reduced productivity time and consequently increased operating costs [9]. Thus, this method is rarely used when machining titanium alloys.

b) Thermally Assisted Machining: In this process, the precise coordination between the cutting tool and an externally controlled heating source, such as laser heating, is needed. The heat source is used to raise the surface temperature and soften the workpiece ahead of the machining point. Due to the thermal softening, the material strength and hardness decrease as temperature increases, thus cutting forces are reduced and material can be removed more easily. However, the precise coordination between cutting tool and heating source must be ensured to avoid overheating and degradation of cutting tool. Additionally, localized melting procedures may result to alloy contamination and equipment damage [4,9].

c) Vibration Assisted Machining: No machining system is perfectly rigid as vibration is always present between the tool and workpiece during machining. However, there is higher chance for vibration to occur during machining of titanium alloys due to the self-excited vibration caused by localized shearing between the workpiece and the cutting tool. This vibration produces surface waviness during the first cut and generation of cyclic forces in the succeeding cuts. The use of a vibration analysis kit allows the reduction of chatter and cyclic forces even at higher speed, resulting to the elimination of chip thickness variation. The kit helps identify the machining conditions at which there is absence of chatter and chip thickness variation [4,9].

d) Application of Liquid Coolant: Cutting fluids address the high temperature and stresses developed at the tool cutting edge during machining. The liquid coolant can lower the cutting temperature generated by 30% and reduce the cutting forces between chip and tool through lubricating action, thereby reducing tool wear rate. Additionally, it removes wear by flushing away the chips from the cutting tool and workpiece interface. The efficiency of heat removal process depends on the heat transfer coefficient between the coolant and the cutting zone. Thus, to improve the effectiveness of the cooling process, several techniques have been developed to control the cutting zone temperature such as cryogenic cooling, minimum quantity lubrication, near dry machining and the use of compressed air or gases [4,9].

e) Hybrid Machining: Hybrid machining entails the combination of one or more techniques to produce machined parts in a more efficient and productive manner. The combination helps highlight the advantages and reduce the drawbacks of certain techniques. However, there is little information available on the hybrid machining of titanium alloys [9].

f) Application of Coatings: The application of coating on the surface of a cutting tool has greatly improved the machining processes by extending the tool life and enhancing the cutting tool performance, especially for difficult-to-machine materials. Coatings improve the properties such as increased hardness, oxidation resistance, toughness and thermal stability, while reducing the coefficient of friction. Additionally, the coatings can be tailored to fit a specific application and be designed in a multilayered structured to further improve the performance. There are several coating systems available which are produced in a variety of methods such as physical vapor deposition (PVD) and chemical vapor deposition (CVD) [10].

g) Use of Solid Lubricant: Machining with solid lubricants is another technique to avoid the use of coolants during operation. Solid lubricants assist machining operations through their lamellar structure. The lamellas orient parallel to the surface in the direction of motion and help prevent contact between surfaces by shearing over each other resulting in reduced friction. The most used solid lubricants are graphite and molybdenum disulphide (MoS_2) [24].

In the machining industry, there is a high volume of liquid coolants used for lubrication and cooling purposes. According to Abdalla et al. [25], the estimated annual usage of cooling lubricant by the European Union is around 320,000 tonnes, out of which 66% need to be disposed. Despite the mechanical advantages, the use of liquid coolants during machining is associated with economic, environmental and health difficulties. The cost of cutting fluid is approximately 7% to 17% of the total machining process cost [24]. Since cutting fluid is continuously needed during machining, the operational and disposal cost would significantly impact the total manufacturing cost of the product. Aside from the financial impact, the disposal of cutting fluids can lead to serious ecological damage and contamination, if not handled properly [19]. The use of liquid coolants also have harmful effects to the operators. Studies have shown that 80% of occupational skin diseases are caused by exposure to liquid coolants. These issues prompted the investigation on the use of biodegradable liquid coolants and its reduction or complete removal during machining [26].

The shift towards sustainable machining can offer both financial and environmental benefits. The reduction or even complete elimination of liquid coolant during machining operation can only be made possible if the alternative method can deliver the functions typically met by the liquid coolants. Dry machining is considered as the best approach to machine components without the aid of cutting fluid which could result to reduced operational costs and environment and health hazards [11]. However, the absence of liquid coolant in dry machining usually results to higher temperature in the cutting zone which could lead to shorter tool life and poor surface geometry and quality [2,24]. Since cutting tool materials usually lose their hardness at elevated temperatures, the high temperature at the cutting zone causes softening of the tool cutting edge which may lead to sudden tool failure. The high temperature can also trigger the chemical reaction between the tool and chip which could further accelerate tool wear. It is difficult to achieve a highly geometrically accurate machined part due to significant heat retention in the workpiece which causes thermal deformation and microstructural changes. Additionally, the technique may also result in the development of residual stresses which could affect fatigue and corrosion resistance. Thus, the main requirements of a cutting tool in dry machining condition are to resist high stresses and retain material hardness at higher operating temperature to have improved wear and oxidation resistance [19].

As previously stated, machining at low speed is not a practical choice to reduce cutting temperature as this will result to lower productivity and increased manufacturing cost [12]. Thus, the development of high-performance wear resistant hard coatings with good thermal stability has become crucial to address the high operating temperature in dry machining, especially for conditions involving difficult-to-machine materials such as titanium alloys. Hard surface coatings based on the transition metal nitrides have been introduced to the market as anti-wear coatings in the early 1970s. One of the most popular and easily available coatings for industrial applications, such as cutting and forming tools, is the titanium nitride (TiN) since it can satisfy most of the coating requirements including high surface hardness, remarkable corrosion resistance and electrical conductivity [27-28]. For several decades, TiN coatings have been deposited on tools, dies and machine-driven components to improve the mechanical performance and life cycle of the material during operation. Commonly produced by PVD or CVD techniques, TiN coating adopts an NaCl crystal structure and exists as a solid solution containing nitrogen in the range of 37.5 at.% to 50 at.% [13].

Although TiN coating delivers good performance in room temperature conditions, it performs poorly under high cutting temperature due to its limited oxidation resistance and inadequate thermal stability [27-28]. The coating tends to lose its inherent promising characteristics when subjected to temperatures above 500°C. When subjected to higher machining speed with the presence of liquid coolant, the corrosion resistance of TiN coating decreases significantly due to the increased machining temperature. Even for dry machining at lower machining speed, the low oxidation resistance of TiN is not suitable for this condition as the operating temperature may range from 700°C to 1000°C due to the absence of liquid coolant [18-19]. Additionally, despite being widely used in various tribological applications by providing a wear resistant surface to protect the underlying substrate, TiN is not considered as a low friction coating material. It has been reported in unlubricated tribological tests that the coefficient of friction of this coating system ranges from 0.3 to 0.9, depending on test geometry, counterpart materials and other parameters [29]. Several studies have been carried out to address the oxidation resistance, thermal stability and high coefficient of friction of TiN coating system to maximize its use as a hard surface coating in numerous applications.

2.5 Development of monolayer TiAlN and TiAlCN coatings

With the aim of addressing the shortcomings of low oxidation resistance and higher coefficient of friction, different alloying elements were introduced to the TiN structure to improve the mechanical and tribological coating performance. Several studies have reported that the addition of aluminum (Al) to form TiAlN can improve the hardness, oxidation resistance and thermal stability of TiN at elevated temperatures while the addition of carbon (C) to form titanium carbon nitride (TiCN) can lower the coefficient of friction [13-18,30]. Therefore, it is expected that a quaternary TiAlCN coating would display a combination of high thermal stability, improved mechanical properties and reduced friction coefficient.

The addition of Al in the cubic NaCl-type TiN structure leads to the formation of TiAlN metastable solid solution [18]. TiAlN has higher oxidation resistance as compared with TiN wherein TiN starts to oxidize at temperature above 500°C while TiAlN displays resistance to oxidation up to 800°C. The high temperature stability is driven by the formation of a dense, highly adhesive protective layer of Al_2O_3 which prevents the diffusion of oxygen into the coating structure [13]. According to the study of Paldey and Deevi [13], the initiation of oxidation depends on Al content, wherein a higher oxidation resistance is expected at higher Al content. Qi et al. [31] fabricated TiAlN coatings via arc ion plating and investigated the oxidation behavior of the film from 25°C to 900°C. The $Ti_{0.34}Al_{0.66}N$ coating reported an onset of significant oxidation above 800°C with the top oxide layer consisting almost completely of Al_2O_3. Zhou et al. [32] deposited TiAlN coatings via magnetron sputtering with 0 to 0.6 Al concentration. For pure TiN, the oxidation started at 550°C in air while the $Ti_{1-x}Al_xN$ coatings began to oxidize at higher temperature. The TiAlN coatings containing 60 mol% Al exhibited excellent resistance to oxidation up to 950°C. These studies confirmed the higher oxidation resistance of TiAlN as compared with TiN coating. Despite the improvement in oxidation resistance and thermal stability, the addition of Al leads to higher coefficient of friction and reduced toughness of the TiAlN coating compared with TiN [16]. In the study of Chang et al. [33], the TiAlN coatings developed by high-power impulse magnetron sputtering (HiPIMS) reported friction coefficient values between 0.68 and 0.77. Yoon et al. [34] developed TiN and TiAlN coatings prepared by arc ion plating technique and compared the friction coefficient of the coatings against steel ball during ball-on-disk wear test. The study reported higher friction coefficient of TiAlN compared with TiN.

Another approach to improve the properties of TiN is the addition of C atoms which results to improved hardness and reduced friction coefficient value at the tool-workpiece interface. It has been reported that TiCN is a solid solution of TiN and TiC which combines the characteristics of both coatings [35]. Hernández-Sierra et al. [36] investigated the behavior of TiN and TiCN coatings on steel deposited by cathodic arc evaporation. The study reported higher hardness for TiCN at 12.2 – 14.9 GPa compared with TiN at 8 – 11.3 GPa. Under dry and lubricated conditions, the friction coefficient values of TiCN were reported to be lower than TiN as the presence of C acts as a solid lubricant which causes the reduction of friction and consequently wear. Despite the improvement in mechanical and tribological properties, TiCN has low oxidation resistance which limits its application at high temperatures. The tribological characteristics of TiCN coating at elevated temperatures were investigated in the study of Polcar et al. [35]. The TiCN samples deposited by unbalanced magnetron sputtering exhibited an oxidation resistance only up to 300°C. Below 200°C, the dominant wear mechanism was plastic deformation. At 300°C to 500°C, fracture, delamination and oxidative wear were the major wear mechanisms. As the temperature increased, the friction coefficient and wear rate also increased.

To eliminate the individual drawbacks of Al and C, both alloying elements were added to TiN structure. Quaternary TiAlCN combines the mechanical properties of TiAlN and TiCN thereby exhibiting a combination of excellent tribological properties and high thermal stability [15-16]. The study of Rashidi et al. [15] reported notably lower friction coefficient values of steel substrate coated with TiAlCN compared with uncoated substrates in the same sliding conditions. The remarkable coefficient of friction values of ~0.17 to ~0.35 were attributed to the presence of an amorphous carbon phase, which acted as a lubricant in between the coating surface and workpiece. Lei et al. [37] concluded that the addition of C in TiAlN would result to: (1) substitutional solid solution, (2) C – C bond formation, and (3) carbides formation. The solid solution strengthening effect of either C or Al atoms in the TiN structure contributes to the superior hardness of TiAlCN compared with TiAlN. This conclusion was supported by the results of the study where TiAlN reported a hardness of 36.6 GPa while TiAlCN hardness at different C concentrations varied between 37.9 GPa to 40.4 GPa. Additionally, the coefficient of friction of TiAlCN coating was reported to be lower than TiAlN.

The deposition technique, concentration of alloying elements and different sources of C atoms on have a huge impact on the structural, mechanical and tribological properties of TiAlCN coatings [16]. A study by Zhang et al. [30] deposited TiAlCN coatings by direct current reactive magnetron sputtering with varying Al content made possible by using different Al/Ti target power ratio. The results show that the addition of Al first leads to increasing coating hardness driven by strengthening effect of the crystal refinement. However, as the Al content is further increased, a dramatic decrease in hardness can be observed due to coarsening of grain size. Crystallite size of 10 – 20 nm reported a hardness value of 33 GPa for the TiAlN coating with 12 at.% Al. The same sample reported the highest friction resistance with a friction coefficient value of 0.25 and low wear rate of 8 x 10^{-6} μm^3/mm N.

Zhang et al. [38] also investigated the effect of varying C concentration to the structure, hardness and tribological performance of TiAlCN coatings prepared using DC magnetron sputtering. At low C concentration, the atoms exist as solid solution in the TiAlN structure thereby producing large columnar structure and coarse surface which results to low hardness and relatively high friction coefficient values. As the C concentration is increased, the grain size decreases since the C atoms decrease the diffusivity on the coating surface during deposition. The grain size refinement result to increase in hardness. From a friction coefficient of 0.8 at 11.6 at.%, the value significantly dropped to 0.19 at C content of 26.7 at.%. As previously stated, the amorphous C phase can act as a solid lubricant between the sliding parts, thereby reducing the friction coefficient. Similar findings on the effect of C concentration on the hardness and friction coefficient of TiAlCN coating were reported by Sahul et al. [18]. However, the study highlighted the decrease in coating hardness with further increase in C which is probably related to the creation of amorphous C phase. Thus, it is essential to identify the optimum C content to deliver exceptional mechanical performance. Aside from Al and C, the N content in TiAlCN can also affect the structure and mechanical properties of the coating. Zeng et al. [39] investigated the optimal N content of TiAlCN coating deposited via radio frequency magnetron sputtering. The study reported that the phases and mechanical properties of the coating exhibited a strong dependence on the N content.

2.6 Advantages of Multilayered TiAlN and TiAlCN coatings

In monolayered coatings, the increase in hardness usually results to brittleness and reduced yield strength. Once there is crack formation, the crack propagates directly to the substrate without any hindrance, followed by subsequent coating failure. This issue is addressed by developing a multilayered structure that can act as an inhibitor to the propagation of cracks developed under the exerted loads during repetitive cutting impacts [13]. Multilayered coatings are composed of several layers of the same or different coating materials stacked in various combinations. The thickness of the individual layer can vary from a few nanometers to 100 nm.

Aside from increasing the capacity to resist fatigue failures by providing a high resistance to the formation and development of fatigue cracks, a multilayered structure can improve the following mechanical properties:

i. The numerous interfaces created between individual layers can further improve the hardness and strength of the coating. The multiple layers allow distribution of stress among the components to avoid catastrophic failure [13].

ii. Lower residual stress present in the film [37,40].

iii. Significantly reduce the physical and chemical activity between the cutting tool and machined material [40].

iv. Prevent heat from friction heat sources to flow to the cutting tool and machined surface, as well as deter diffusion processes to occur at the cutting tool-workpiece interface [40].

The multilayered configuration enables the formation of different material combination which combines the advantages of individual components. The opportunity to vary the multilayer architecture based on the desired application can result in the optimization of mechanical and tribological properties, as well as ensure chemical stability of the coating material [13].

It has been reported by numerous studies that the multilayered coating configuration exhibits superior mechanical and tribological properties compared with the monolayered coatings. The TiAlN/TiAlCN coating developed by Tillmann et al. [16] by hybrid DCMS and HiPIMS exhibited superior hardness and wear resistance compared with monolayered TiAlN coating. TiAlN reported 24 GPa hardness while TiAlN/TiAlCN reported higher hardness at 28 GPa. A similar multilayered configuration was developed by AL-Bukhaiti et al. [41] by magnetron sputtering. The multilayered coated steel substrate exhibited a friction coefficient of 0.25 and 0.35 against Al_2O_3 and 100Cr6 steel balls, respectively. These values were three times lower than the friction coefficient values of uncoated substrate at 0.77 and 0.85 against Al_2O_3 and 100Cr6 steel balls, respectively. Lei et al. [37] investigated the effect of partial pressure to the mechanical properties of the same TiAlN/TiAlCN coatings structure deposited by multi-arc ion plating method. The results showed an excellent adhesion strength of 52 N and minimal friction coefficient value of 0.46.

Rizzo et al. [42] analyzed the effect of multilayer architecture on the thermal and tribological properties of TiAlN/AlN coating prepared by reactive magnetron sputtering. The coating exhibited excellent oxidation resistance and thermal stability at 900°C. Compared with the monolayered structure, the multilayered coatings exhibited better wear resistance properties due to the presence of interfaces which act as obstacles to crack propagation. The friction coefficient reported for TiAlN/AlN at 400°C was at 0.33 compared with 0.53 for the monolayer. Kawata et al. [43] reported that the multilayered coatings TiAlN/TiN, TiAlCN/TiAlN/TiN and TiAlON/TiAlN/TiN prepared by pulse-enhanced CVD exhibited resistance to oxidation up to 800°C. The high oxidation resistance is due to the formation of a stable Al_2O_3 layer which prevented further oxidation to occur. The ball-on-disk test reported that the TiAlCN/TiAlN/TiN coating has the lowest friction coefficient at 0.44 which is due to the increased hardness and lubricity by the addition of C. The oxidation resistance and tribological properties of the multilayered coatings were reported to be better than the monolayered TiN coating. Similar with monolayered coatings, the concentration of alloying elements can also significantly impact the structure and properties of multilayered coatings. Chen at al. [44] developed TiAlCN/TiAlN/TiAl multilayered coatings by cathodic vacuum arc technique with various C concentration and reported that an optimized amorphous C phase is needed to exhibit high hardness and excellent tribocorrosion performance.

2.7 Dry Condition Machining Performance

Aside from the basic characterization and tribological tests to assess the properties of newly developed coatings, it is useful to determine the actual performance when applied on the surface of a cutting tool used in machining operations. Studies have reported that monolayered and multilayered coatings based on TiAlN and TiAlCN showed promising hardness, wear and corrosion resistance under dry machining conditions.

Jindal et al. [45] deposited TiAlN and TiCN coatings on WC-6wt%Co alloy by PVD and evaluated the cutting performance via turning of Inconel 718, carbon steel and cast iron. TiAlN and TiCN performed significantly better than tools coated in TiN on all three workpieces. TiAlN exhibited the lowest maximum flank wear, nose wear and crater wear. Sharif and Rahim [46] performed drilling tests at various cutting speeds on Ti6Al4V using carbide twist drills coated with TiAlN. Both uncoated and coated drills experienced similar modes of failure including non-uniform flank wear, chipping and catastrophic failure. However, TiAlN coated drill exhibited an outstanding tool life and lasted for 7.8 min at cutting speed of 25 m/min while the uncoated drill recorded a short tool life of 0.31 min. This suggests that the TiAlN coating protected the tool and managed to substantially reduce the wear rate of the cutting material. The study of Vereschaka et al. [47] evaluated the turning of steel using carbide tools coated with multilayered Ti/TiCN/TiAlCN coating. The results show that the multilayered coated tools showed better wear resistance than monolayered and uncoated tool. Ti/TiCN/TiAlCN exhibited a tool life of 7 min while monolayer TiN and uncoated tool lasted for 4 min and 3 min, respectively.

Based on the current published studies, the addition of Al and C alloying elements to the TiN structure produces TiAlN and TiAlCN structures that have promising mechanical and tribological performance. Additionally, the mechanical properties and dry machining performance of the multilayered coatings appear to be superior to the monolayered structure. However, there seems to be a limited investigation on the systematic characterization and comparison between the different properties of those coatings. Additionally, majority of the studied coatings are also developed in a laboratory scale, regardless of the deposition technique employed. This study would help understand the behavior of monolayer and multilayer TiAlN and TiAlCN coatings developed in an industrial setup.

CHAPTER 3: EXPERIMENTAL PROCEDURE

The experimental process performed in this study consists of five primary stages as follows: (1) substrates preparation; (2) deposition of industrial optimized TiAlN, TiAlCN and TiAlN/TiAlCN coatings performed at the premises of an enterprise; (3) basic characterization; (4) evaluation of the oxidation resistance and thermal stability; and (5) tribological characterization of the deposited coatings.

3.1 Substrate Preparation

Different types of substrates were utilized for the deposition of the industrial-grade coatings, each for different set of characterization techniques. The coatings were deposited onto Si (111) wafer for cross-section, surface morphology and chemical composition analyses; FeCrAl alloy substrates for the structural analysis, hardness measurements and evaluation of the thermal stability of the coatings; Al_2O_3 substrates for the investigation of oxidation resistance; and steel substrates for adhesion test and tribological performance evaluation at room temperature.

3.2 Deposition of Industrial Coatings

In this thesis, three different industrial-grade coatings were produced: (1) monolithic TiAlN, (2) monolithic TiAlCN and (3) multilayered TiAlCN/TiAlN coatings. The deposition of the coatings was carried out in an industrial CemeCon coating device using DC magnetron sputtering technique. The chamber comprised of several cathodes connected to pulsed DC power supplies: (1) one Ti and three TiAl targets for TiAlN; (2) four TiAlC targets for TiAlCN; and (3) two TiAl and two TiAlC targets for TiAlN/TiAlCN coatings. The chamber was heated to 400°C for 90 min prior to depositions. A combination of pulsed and hollow cathode etching procedures were used for the cleaning and activation of the surface of the substrate before the deposition. Additionally, to improve coating adhesion to the substrate, an adhesion layer of pure Ti was deposited at power density of 2 kW. Table 3.1 summarizes the parameters utilized for the deposition of each industrial coating.

Table 3.1
Main deposition parameters.

Parameter	TiAlN	TiAlCN	TiAlN/TiAlCN
Target	(3) TiAl, (1) Ti	(4) TiAlC	(2) TiAl, (2) TiAlC
Target power (kW)	TiAl – 9.5	(3) TiAlC – 9.5	(2) TiAl – 8
	Ti – 5	(1) TiAlC – 4	(2) TiAlC – 8
Substrate bias voltage (V)	60	60	90
N partial pressure (Pa)	0.58	0.58	0.58
Temperature (°C)	480	480	480
Deposition time (s)	8700	6088	5700
Etching time (s)	3300	6600	3600

As seen from Table 1, TiAlN was deposited for 8700 s powering the TiAl and Ti targets at 9.5 kW and 5 kW, respectively. For TiAlCN, the deposition lasted for 6088 s powering four targets of TiAlC at 9.5 kW (three TiAlC) and 4.5 kW (one TiAlC). Lastly, multilayered TiAlN/TiAlCN was deposited for 5700 s with the following configuration: (1) first layer of TiAlN, applying 8 kW at the TiAl target for 600 s, (2) TiAlN/TiAlCN bilayers using the same power for TiAl and TiAlC targets at 8 kW for 3420 s; and the (3) final layer of TiAlCN deposited for 1680 s powering the TiAlC target at 8 kW. The partial pressure of N was at 0.58 Pa for all coatings while the substrate bias voltages were kept at 60 V and 90 V for the monolithic and multilayered coatings, respectively. Figure 3.1 illustrates the architecture of the deposited coatings.

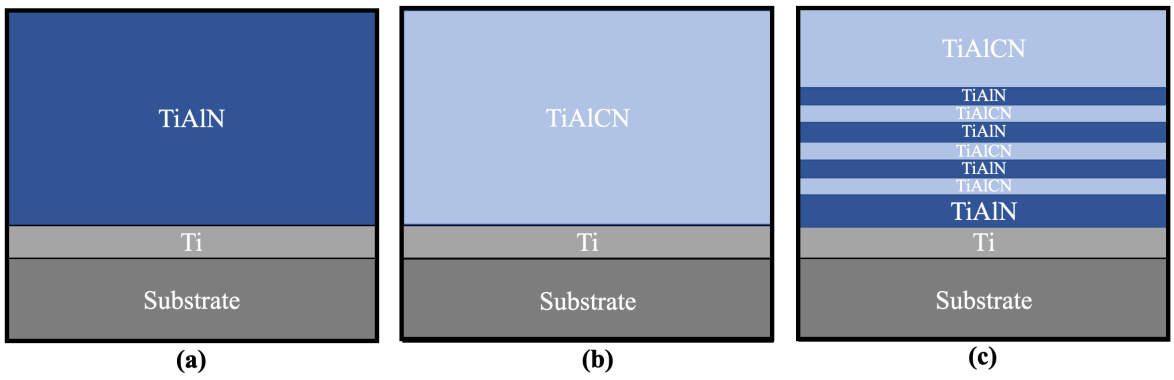

Figure 3.1 Schematic diagram of the architecture of: (a) TiAlN, (b) TiAlCN and (c) TiAlN/TiAlCN industrial coating systems

3.3 Basic Characterization

The cross-section, surface morphology and thickness of the coatings were investigated using scanning electron microscopy (SEM) while the chemical composition was determined using energy dispersive spectroscopy (EDS). The crystallographic structure of the coatings was evaluated using X-ray diffraction (XRD) by an X'Pert Pro MPD diffractometer with Cu Kα1 radiation at 45 kV and 40 mA. The diffractograms were acquired using conventional and grazing incidence modes in the 2θ range of 20° to 80°. XRD patterns acquired from grazing incidence mode were used to calculate the lattice parameter and average grain size while patterns obtained in conventional mode were used to determine the preferential orientation.

The adhesion between the substrate-coating interface is crucial to ensure good performance during service and was evaluated by scratching the surface with a linearly increasing force from 5 N to 70 N. A Rockwell C indenter with a spherical tip of 0.2 mm radius was used to scratch the surface at a speed of 10 mm/min and loading speed of 100 N/min. The scratches and failure mode were investigated using an optical microscope and the critical loads were determined using the scratch test standard [48]. The hardness (H) and Young's modulus (E) values of the as-deposited films were measured by nano-indentation technique using a Berkovich diamond pyramid indenter at 15 mN applied load. The indentation depth was kept at less than 10% of the film thickness to eliminate the effect of the substrate on the measurement.

3.4 Oxidation Resistance and Thermal Stability

Coatings deposited on Al_2O_3 were subjected to thermogravimetric analysis (TGA) to study the oxidation resistance. The coatings were first heated from room temperature up to 1100°C at 20°C/min rate to determine the onset point of oxidation. Using a micro-balance attached to the equipment, the oxidation mass gain was evaluated at 2 s intervals. The coatings were then subjected to isothermal oxidation tests for 2 h. The isothermal temperature was selected based on the onset point of oxidation curves. The oxide phases formed were characterized by XRD and the distribution of the main elements characterized by SEM-EDS. To investigate the thermal stability, the samples were annealed at 800°C in an oven under Ar + H (95% Ar + 5% H) atmosphere, for 2 h. The changes on the structure and mechanical properties of the coatings were evaluated by XRD and hardness tests.

3.5 Tribological Test

A room temperature pin-on-disk tribometer was used to evaluate the tribological performance of the coatings against Al_2O_3 counterpart. All the tests were performed without lubrication at a constant radius of 8 mm and 0.1 m/s sliding velocity. Table 3.2 summarizes the major parameters employed during the tribological test for all industrial coatings.

Table 3.2
Pin-on-disk test main parameters.

Test	Load	Cycle
1	10	10,000
2	5	20,000
3	5	10,000

Normal load and number of cycles were two magnitudes varied in the tests. For normal load, 10 N and 5 N loads were used to mimic two different contact pressure conditions, with maximum values at 0.83 GPa and 0.67 GPa, respectively, that coated components need to withstand during operation. Comparison of the different number of cycles can also help evaluate the longevity of the coating performance which can impact material and time resources during actual application. Additionally, these parameters allowed for the direct comparison with other studies on hard coatings.

The evolution of coefficient of friction (COF) was continuously acquired during the tests. The wear track cross-sectional 2D profiles were acquired using a 2D profilometer and the specific wear rate was calculated through the determination of the wear volumes using Archard's Law [49]. Wear mechanisms taking place on the wear tracks were analyzed by SEM and the presence of wear debris on the coating surface was characterized using EDS. Additionally, the wear scar on the Al_2O_3 counterpart was evaluated using optical microscope.

CHAPTER 4: RESULTS AND DISCUSSION

4.1 Chemical Composition

The chemical compositions of TiAlN, TiAlCN and TiAlN/TiAlCN coatings as measured by EDS are shown in Table 4.1. N content for all coatings is approximately the same at 48 at.%, confirming that quasi-stoichiometric coatings were produced. TiAlN displayed high content of Al at 30.7 at.% while the Ti content is lower at 20.7 at.%. TiAlCN and TiAlN/TiAlCN reported a reverse relationship; low Al content at 7.5 – 8.1 at.% and higher Ti content at 37.7 – 38 at.%. The significant difference in the Ti/Al ratio is attributed to: (1) variation of target configuration in the chamber; (2) different chemical composition of targets; and (3) different power applied to the different targets during deposition. The C concentration for TiAlCN is 6.6 at.% while the global C concentration in TiAlN/TiAlCN is 5.5 at.%.

Table 4.1
Chemical composition of the coatings measured by EDS.

Sample	N at.%	Ti at.%	Al at.%	C at.%	Ti / Al
TiAlN	48.6 ± 0.2	20.7 ± 0.1	30.7 ± 0.1	-	0.67
TiAlCN	48.2 ± 0.1	37.7 ± 0.1	7.5 ± 0.1	6.6 ± 0.2	5.02
TiAlN/TiAlCN	48.4 ± 0.4	38.0 ± 0.1	8.1 ± 0.1	5.5 ± 0.2	4.70

4.2 Structure and Morphology of the Coatings

Figure 4.1 shows the XRD diffractograms of the as-deposited coatings acquired in conventional mode. All coatings were indexed to face centered cubic (fcc) NaCl type structure. TiAlN exhibited a (200) preferential growth while TiAlCN and TiAlN/TiAlCN exhibited (111) preferential growth. The peaks at 44.4° and 64.5° correspond to peaks assigned to the substrate; while a low intensity Ti peak originated from the Ti adhesion layer in TiAlCN can be detected at 38.4°.

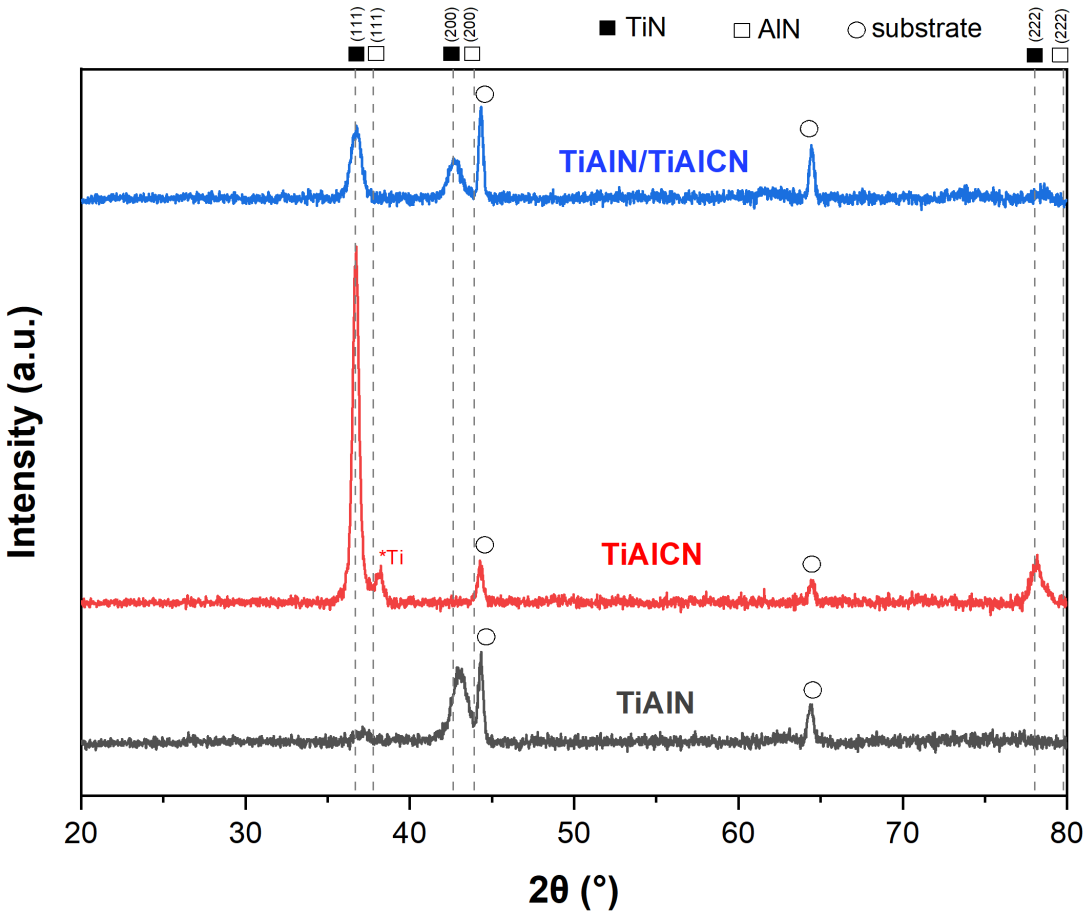

Figure 4.1 XRD diffractograms of as-deposited coatings.

The addition of Al atoms replaces Ti atoms in the TiN crystal structure to form TiAlN [30]. In this study, the TiAlN peaks are placed in between the TiN (ICDD 01-71-0299) and the AlN (ICDD 00-025-1495) reference diffraction cards. The reduction in d-spacing in relation to the TiN card is due to the substitution of Ti atoms by Al atoms which have a lower atomic radius. This result agrees with those from literature, where TiAlN coatings is a substitutional solid solution that keeps the fcc NaCl type structure but with lower lattice parameter compared with TiN [32]. This finding is confirmed by the calculated values of d-spacing and lattice parameters based on (111) and (200) peaks as shown in Table 4.2. TiAlN exhibited lower lattice parameter values of 0.416 nm for (111) and 0.4179 nm for (222) compared with the standard TiN at 0.4239 nm. Nevertheless, the presence of tensile and/or compressive residual stresses should not be discarded for the position of the XRD diffraction peaks, as compressive and tensile stresses push the XRD diffraction peaks to lower and higher angles, respectively [30]. In this thesis, the evaluation of such magnitude was not possible.

On the other hand, it can be observed that the peaks of TiAlCN and TiAlN/TiAlCN coatings shifted towards lower diffraction angles with respect to TiAlN peaks, suggesting lattice expansion. This increase in lattice can be due to: (1) different chemical composition of the coatings [30,38]; (2) addition of C atoms in the TiAlN lattice [50]; and (3) different level of stresses on the films [16,51]. For (111) dominant peak, TiAlCN and TiAlN/TiAlCN reported 0.4234 nm and 0.4228 nm lattice parameter values, respectively. The d-spacing and lattice parameter values of these coatings are higher than TiAlN but lower than the TiN from the reference card, as shown in Table 4.2.

Table 4.2
Calculated values of d-spacing and lattice parameters.

Sample	d-spacing [nm]		Lattice parameter [nm]	
	(111)	(200)	(111)	(200)
TiN*	0.2447	0.2120	0.4239	0.4239
TiAlN	0.2402	0.2090	0.4160	0.4179
TiAlCN	0.2444	0.2111	0.4234	0.4216
TiAlN/TiAlCN	0.2441	0.2112	0.4228	0.4237

*ICDD card no. 01-071-0299

Figure 4.2 shows the average crystallite size calculated using Scherrer equation based on the full width at half maximum (FWHM) of the (111) and (200) peaks. TiAlN reported the smallest average crystallite size while TiAlCN exhibited the largest average crystallite size. Tillman et al. [16] reported a decrease in average crystallite size upon the inclusion of C to the TiAlN structure which is a result of grain refinement. However, in this study, the opposite trend is observed wherein the average crystallite sizes of TiAlCN and TiAlN/TiAlCN are higher than TiAlN. A recent study by Chen et al. [44] exhibited the same trend on increase in average crystallite size with carbon content. The results reported average crystallite size values of 29.9 nm, 32.75 nm and 32.2 nm for C content at 0 at.%, 8.6 at.% and 12.4 at%, respectively. It must be noted that the industrial coatings were developed at different deposition parameters, thus, the C content is not the only factor that have affected the difference in average crystallite size.

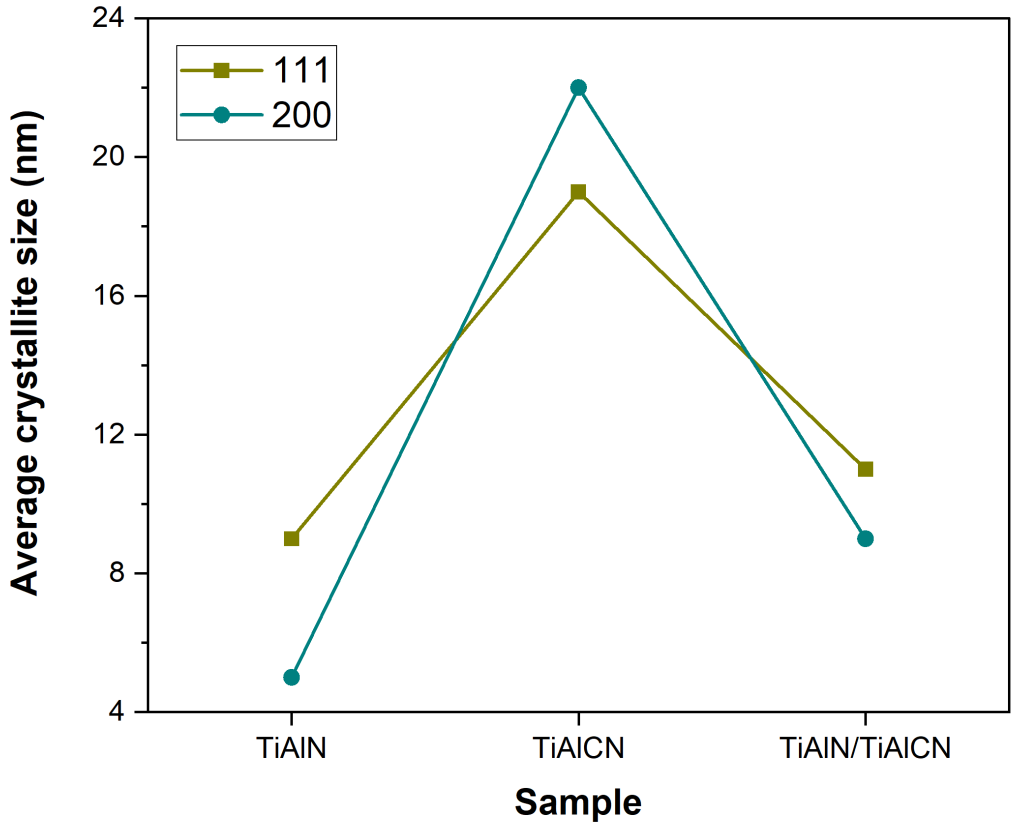

Figure 4.2 Average crystallite size of as-deposited coatings.

Figure 4.3 shows the SEM micrographs of the cross-section and surface morphology of the as-deposited TiAlN, TiAlCN and TiAlN/TiAlCN coatings. The micrographs exhibited a columnar growth for the cross-section, extending from substrate up to the surface of the coating at an increasing diameter with a typical cauliflower-like surface morphology. The thickness of the coatings is 4.2 µm and 2.4 µm for monolithic and multilayered coatings, respectively. The lower thickness of the multilayered coating is mainly due to lower deposition time compared with the monolayered coatings.

Chang et al. [33] attributed the transition from a well-defined columnar structure to a denser cross-section to the increase in Al/(Al + Ti) atomic ratio in the coating. This finding corroborates the results of this study wherein the highest Al atomic ratio at 0.60 is obtained by TiAlN with the densest cross-sectional structure, as seen in Figure 4.3a. Additionally, the higher power density of the targets used for TiAlN deposition led to the formation of a high number of heterogeneous nucleation sites and less visible columnar structure. The Ti interlayer boundary is not visible in the micrographs.

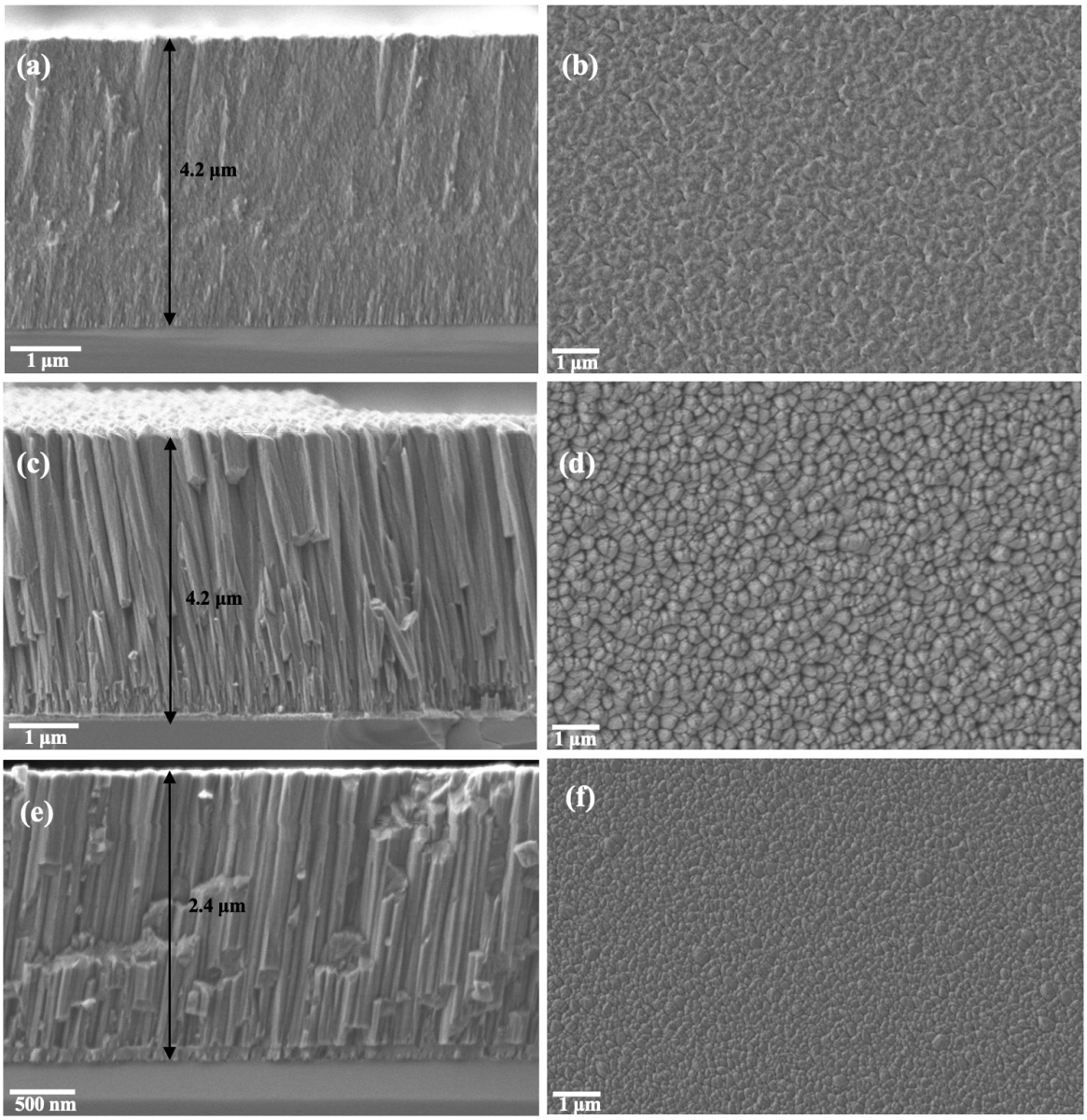

Figure 4.3 SEM micrographs of the cross-section and surface morphology of as-deposited coatings: (a – b) TiAlN, (c – d) TiAlCN and (e – f) TiAlN/TiAlCN.

4.3 Adhesion Strength

The adhesion strength of the as-deposited coatings onto steel substrate was evaluated by determining the critical loads: L_{C1}, L_{C2}, and L_{C3} correspond to the first crack event, first delamination of the coating coupled with substrate exposure and full coating delamination, respectively [52]. The failure mode type upon scratch test was also investigated. Figure 4.4 shows the scratch track for the coatings deposited onto steel substrate observed using an optical microscope.

In general, the scratch tests revealed that all coatings have remarkable adhesion strength. The TiAlN/TiAlCN exhibited the highest L_{C2} at ~51 N with minimal irregular spallation along the edges of the track. Similar features can be found on the TiAlCN scratch track which exhibited ~49 N L_{C2}. Monolithic TiAlN exhibited the lowest L_{C2} at ~40 N with more pronounced spallation along edges of the track. This is mainly caused by mismatch in strain between coating and substrate which imposes shear stress at the interfaces and leads to delamination of the sides of the track. No coating delamination can be observed in any of the magnified scratch tracks. The results show that the multilayered TiAlN/TiAlCN has the best adhesion strength onto a steel substrate.

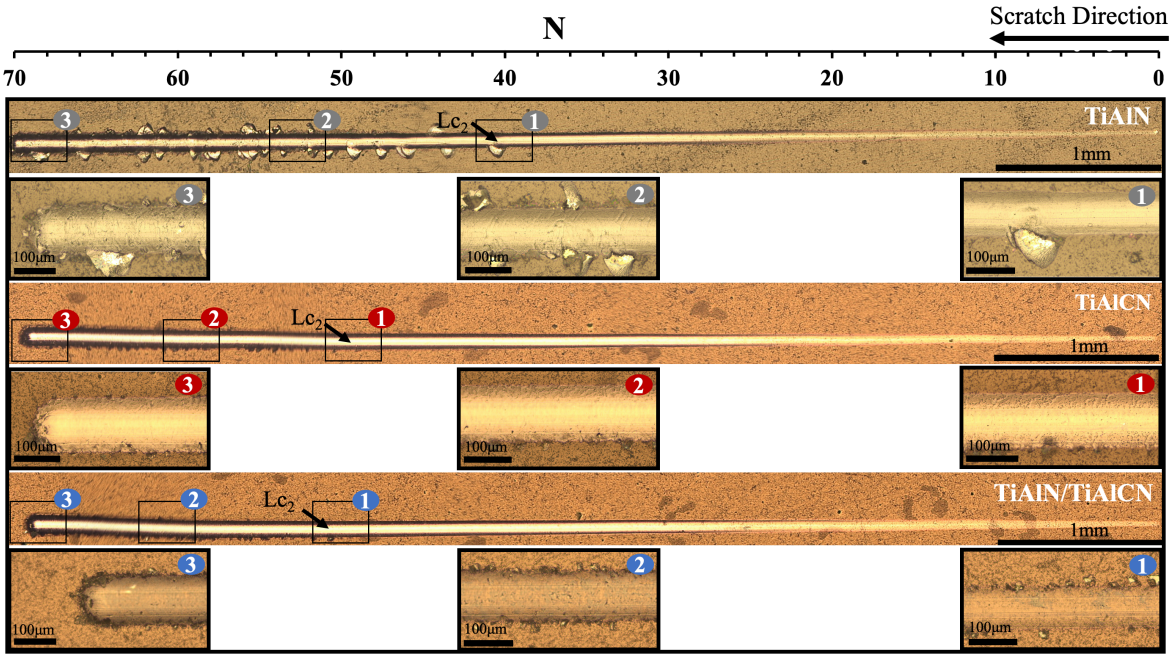

Figure 4.4 Scratch tracks of TiAlN, TiAlCN and TiAlN/TiAlCN on steel substrate

4.4 Oxidation Resistance

Thermogravimetric analysis (TGA) tests were performed to evaluate the onset point of oxidation and oxidation resistance of the coatings. Figure 4.5 displays the results from TGA using industrial air (99.99% purity) by heating up to 1100°C, at a constant ramp rate of 20°C/min and then cooled down to room temperature. Based on the TGA curves, the onset point of oxidation is ~900°C, ~850 °C, and ~800°C for TiAlN, TiAlCN and TiAlN/TiAlCN, respectively.

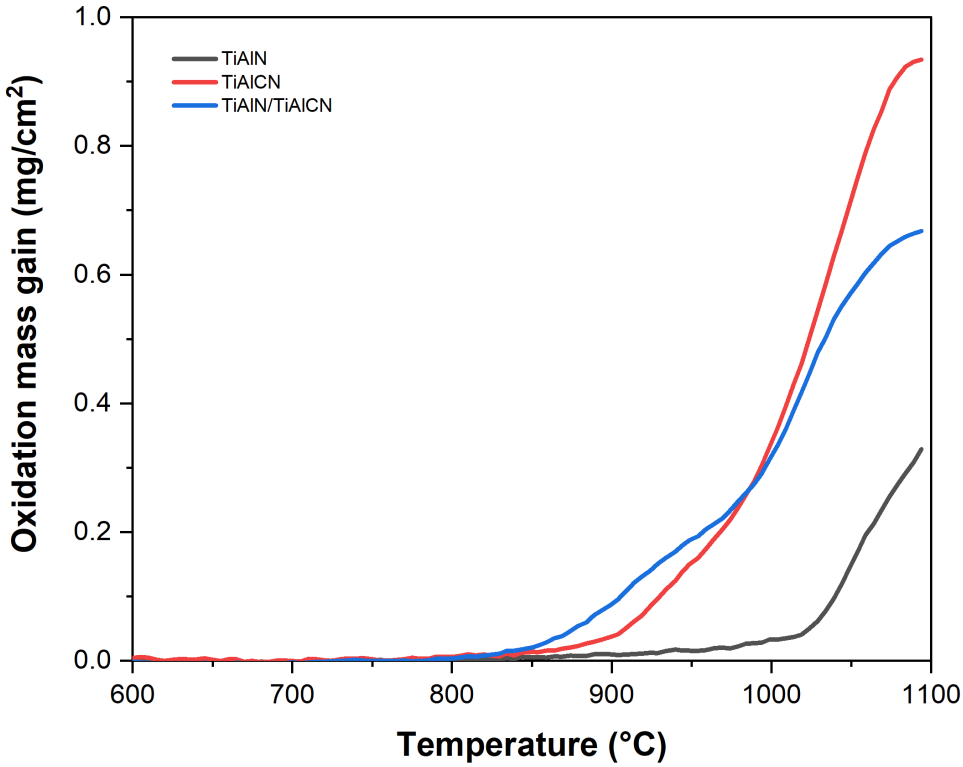

Figure 4.5 Thermogravimetric oxidation curves of the coatings exposed from RT up to 1100°C using a heating rate of 20°C/min.

According to Panjan et. al [53], the remarkable oxidation resistance of TiAlN-based coatings is due to the formation of a thermally stable oxide scale comprised of dense Al_2O_3 upper layer and porous TiO_2 lower layer. The simultaneous diffusion of Al atoms toward the oxide/air interface and the diffusion of oxygen to the oxide/nitride interface, along with N depletion, led to the oxide scale formation. The oxidation resistance strongly depends on the Al/Ti atomic ratio wherein increasing the Al content promotes the formation of Al_2O_3 layer, while the growth rate of the porous and highly permeable TiO_2 layer is reduced [13,53]. Additionally, a dense microstructure tends to suppress the diffusion rates of Al atoms outward and oxygen atoms inward during the oxidation. As previously discussed, the Al content has an impact to the microstructure of TiAlN-based coatings. Thus, with 30.7 at.% of Al and the densest microstructure as seen in Figure 4.3a, TiAlN exhibited the best oxidation resistance among the three coatings with an onset point of oxidation at a high temperature of 900°C. This improved oxidation resistance is further confirmed by the shape of the TiAlN oxidation curve which suggests that the coating was not yet fully oxidized at 1100°C; this is confirmed by SEM cross-section analysis and elemental line profiles along the cross-section morphology.

Due to the low Al content, TiAlCN and TiAlN/TiAlCN have lower onset point of oxidation at 850°C and 800°C, respectively. The oxidation curves increase at a higher rate compared with TiAlN and reach a plateau at 1100°C signifying complete oxidation of the coatings. The formation of oxide layers is confirmed in the SEM and elemental line profile of the cross-section. A study by Peng et al. [54] investigated the combined effect of Al content and structure on the oxidation resistance of TiAlN-based coatings and concluded that coatings with higher Al content and monolithic in structure have better oxidation resistance.

For further comparison of the oxidation resistance, the coatings were isothermally tested at 900°C for 2 h. The corresponding mass gain curves of the different coatings are shown in Figure 4.6. In line with the dynamic oxidation curve, all coatings exhibited mass gain once exposed to 900°C (0 min point); TiAlN reported the lowest mass gain while TiAlN/TiAlCN reported the highest mass gain. The TiAlN coating exhibited minimal and gradual mass gain over time driven by its enhanced resistance to oxidation. For TiAlCN and TiAlN/TiAlCN, the oxidation mass gain curve follows a steep increasing trend for the first 50 min. After this time, the curve reaches a plateau, suggesting that the coatings were fully oxidized.

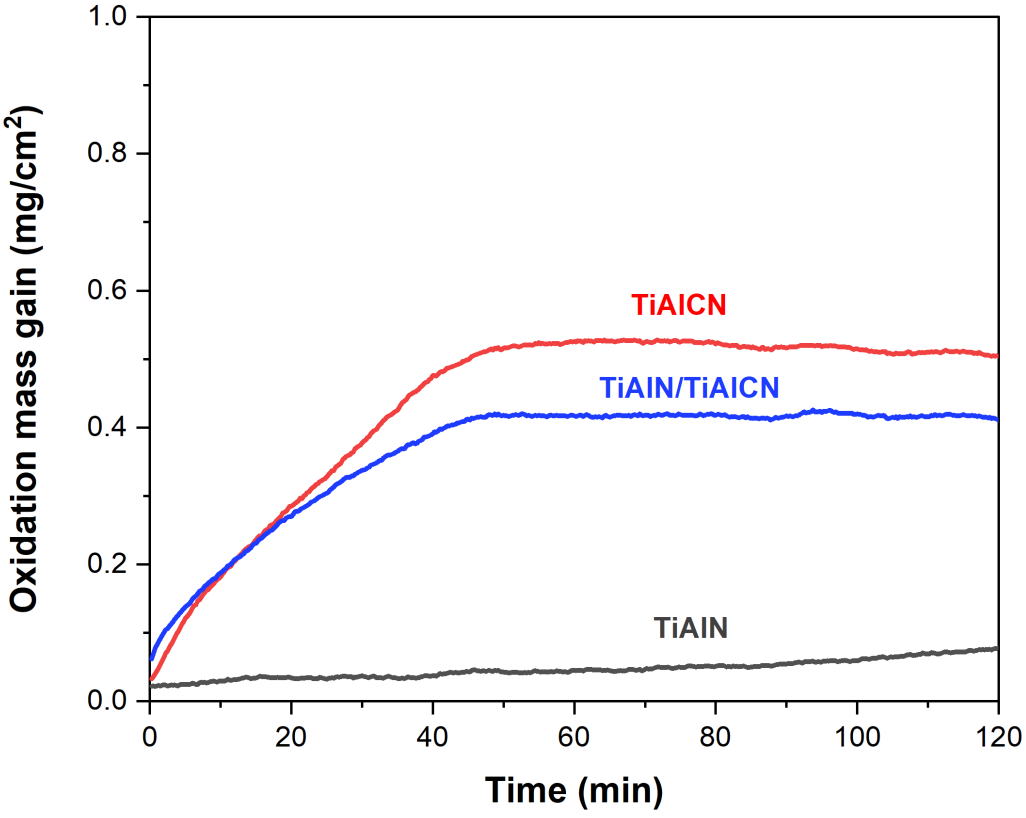

Figure 4.6 Isothermal oxidation curves of TiAlN, TiAlCN and TiAlN/TiAlCN coatings exposed in air at 900°C for 2 h.

The oxide phases formed during isothermal oxidation tests were analyzed by XRD and the results are shown in Figure 4.7. The major peaks for oxidized TiAlN were indexed to Al_2O_3 with a minimal TiO_2 peak at 54.5°. The higher Al content in the TiAlN coating promoted the formation of a layer richer in Al_2O_3 phase [53]. On the other hand, the major peaks in the oxidized TiAlCN and TiAlN/TiAlCN coatings are indexed to Al_2O_3 and rutile-TiO_2 phases. The detection of rutile-TiO_2 may be due to the higher concentration of Ti on the films as compared to TiAlN film. Analysis on the cross-section morphology and elemental map distribution confirm the nature of the oxide scale formation.

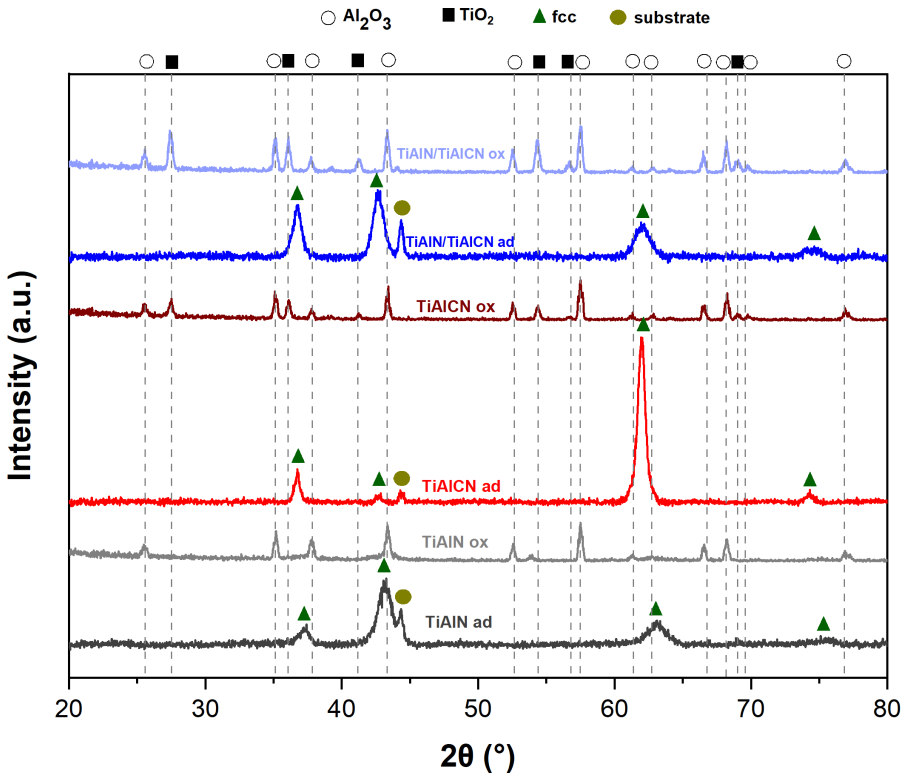

Figure 4.7 XRD diffractograms of as-deposited (-ad) and oxidized (-ox) coatings at 900°C for 2 h

The cross-sectional SEM micrograph and elemental map distribution of the oxidized coatings were acquired to characterize the distribution of the main elements and the extent of formation of the oxide scale. Figure 4.8 confirms the formation of oxide layer on the surface of the monolithic TiAlN coating; however, it is evidently clear that a huge portion of the original coating still exists. This portion of the cross-section is similar to the dense columnar structure of the as-deposited TiAlN shown in Figure 4.3a and corroborates the isothermal test finding that the coating is not yet fully oxidized after the specified oxidation temperature and period.

The elemental map distribution in Figure 4.8 shows the presence of Al and Ti atoms in the oxide layer which confirms the bilayered structure: (1) dense Al_2O_3 layer on top; and (2) porous TiO_2 layer below. However, there is no clear boundary between these two layers. The formation of Al_2O_3 acts as a surface protective layer by: (1) providing a barrier for the diffusion of O from the environment; and (2) preventing the metallic ions and N from diffusing out of the coating [55-56]. This helped improve the oxidation resistance of TiAlN and minimize the oxide scale thickness which validates the low mass gain during oxidation.

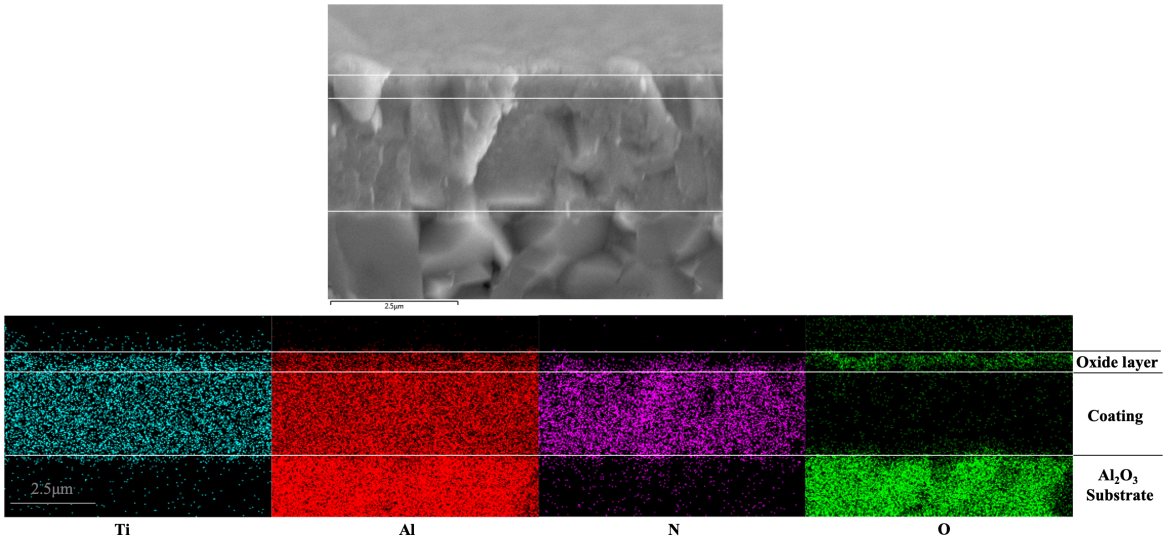

Figure 4.8 Cross-section SEM micrograph and elemental map distribution of oxidized TiAlN coating.

In Figure 4.9, the micrograph and elemental map distribution suggests that the TiAlCN coating has been fully oxidized. The well-defined columnar structure in the cross-section of the as-deposited coating is no longer visible. The elemental map distribution exhibits the presence of Al-rich and Ti-rich bilayer oxide scale, which were also found in the XRD results in Figure 4.7. Due to equipment limitation, there is an energy peak overlap between N-Kα (0.392 keV) and Ti-Lα (0.452 keV) which results to the presence of N signal, despite its absence in a specific region in the coating [7]. Thus, the N atoms detected in the Ti-rich oxide layer can be omitted or be attributed to Ti signal. Unlike the addition of Al atoms, the addition of C atoms is expected to deteriorate the oxidation resistance of the coating [55]. The presence of C and the lower Al content at 7.5 at.% contributed to the complete oxidation of TiAlCN coating which implies a weaker barrier for oxygen diffusion and corroborates the high value of oxidation mass gain reported in the isothermal oxidation curve in Figure 4.6.

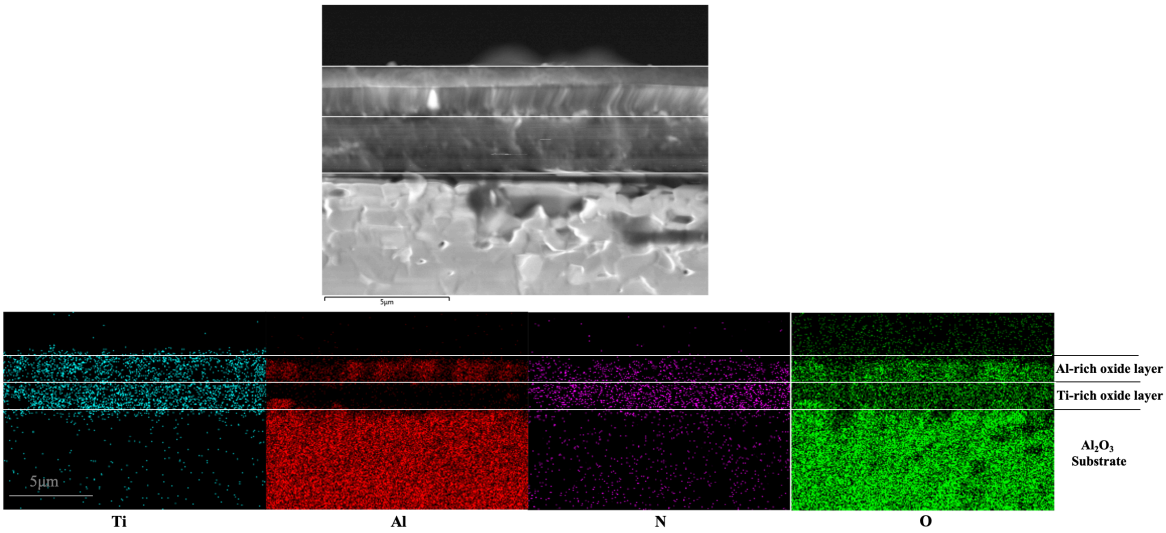

Figure 4.9 Cross-section SEM micrograph and elemental map distribution of oxidized TiAlCN coating.

Similar to TiAlCN, the cross-section SEM micrograph and elemental map distribution for oxidized TiAlN/TiAlCN coating suggests a complete oxidation after being subjected to 900°C for 2 h, as seen in Figure 4.10. The N signal in the oxide layer must be disregarded or attributed to Ti as this is a limitation of the equipment. Instead of a columnar structure, the cross-section morphology of the coating reveals an agglomerated structure. The extent of oxide scale confirms the low oxidation resistance of the coating driven by presence of C and low Al concentration.

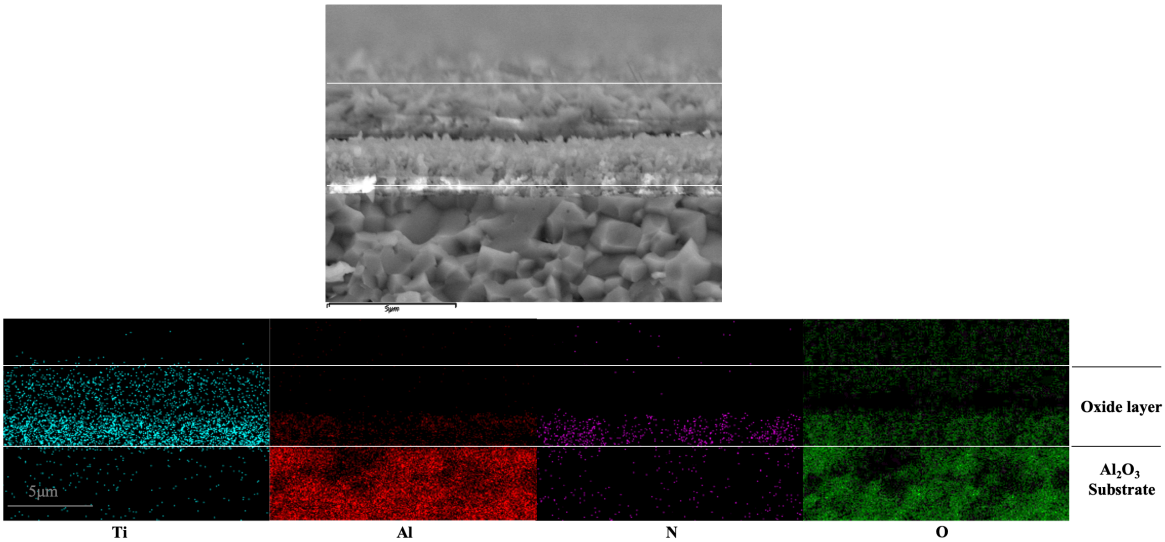

Figure 4.10 Cross-section SEM micrograph and elemental map distribution of oxidized TiAlN/TiAlCN coating.

4.5 Thermal Stability of Coatings

4.5.1 Hardness and Young's Modulus

Figure 4.11 shows the hardness (H) and Young's modulus (E) of the as-deposited and annealed coatings. The multilayered TiAlN/TiAlCN coating exhibited the highest hardness and Young's modulus values (38 GPa and 374 GPa, respectively) among all the coatings. On the other hand, as-deposited TiAlN and TiAlCN reported comparable hardness values at 27 GPa. TiAlCN has a higher Young's modulus at 338 GPa while TiAlN reported the lowest E value at 296 GPa. The as-deposited coatings developed in this study reported similar hardness values compared with other studies of the same coating systems [30-33]. It is difficult to highlight which factor primarily influenced the H and E values as the coatings utilized different parameters during deposition. However, the high hardness of as-deposited TiAlN/TiAlCN can be related to the interfaces present in the multilayered structure which hindered the movement of dislocations [13].

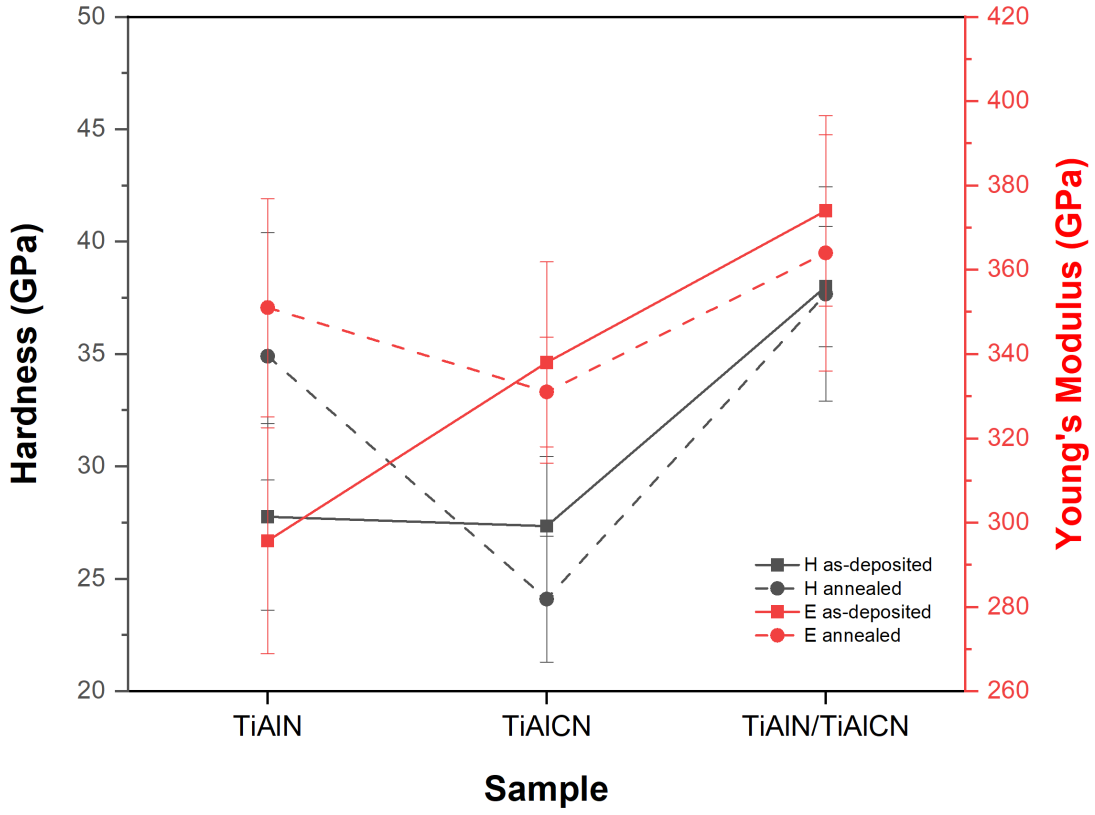

Figure 4.11 Hardness and Young's Modulus of as-deposited and annealed coatings.

The hardness of as-deposited monolithic TiAlN coating can be attributed to the relatively high Al concentration of 30.7 at.% added into the TiN structure. The presence of Al increases volume defects during grain growth which may act as additional obstacles for the dislocation movement, resulting to a higher hardness compared with TiN [30,57]. The separate studies of Lei et al. [37], Zhang et al. [38] and Jang et al. [51] investigated the effect of C addition to the hardness of TiAlCN coatings. According to their results, coating hardness is influenced by C atoms through: (1) increase of covalent bonding in the structure as C reduces the valence electron concentration, (2) solid solution hardening as C atoms exist as solid solution in TiAlN crystal lattice and (3) formation of soft carbon phases once C exceeds its solid solubility. The study of Stueber et al. [50] reported that the soft carbon phases occurs at C content above 8 at.%, which is not applicable in this study. These factors support the comparable hardness of TiAlCN with TiAlN despite the low Al content at 7.5 at.% compared with 30.7 at.% of TiAlN. Upon the addition of C to the TiAlN structure, the Young's modulus values increased. The addition of elements is an influential factor on the coating's mechanical properties; however, it may not be the only contributing factor to this trend.

Annealing treatment generally increases the H and E values of coatings, which can be attributed to the increase in crystallinity. Upon annealing, the H and E values of TiAlN significantly increased to 35 GPa and 352 GPa, respectively. Similar trend can be observed in the study of Bartosik et al. [58] wherein the H and E increases until 900°C before it decreases upon annealing at 1000°C. The Al atomic concentration may influence the onset of c-TiN and w-AlN formation which impacts the hardness values at higher annealing temperatures. On the other hand, for TiAlCN and TiAlN/TiAlCN, a minimal decrease in H and E values can be observed after annealing. The study of Shtansky et al. [59] which investigated the thermal stability of TiAlCN coatings until 1200°C, concluded that the decrease in hardness at 800°C is due to spinodal decomposition.

4.5.2 Crystalline Structure

Figure 4.12 shows the XRD diffractograms of as-deposited and annealed coatings at 800°C for 2 h. The annealed coatings show no major peak changes which are still indexed to fcc NaCl type structure, similar to the as-deposited coatings. The dominant orientation for TiAlN is (111) while the dominant orientation for TiAlCN and TiAlN/TiAlCN is (200). The peaks at 44.4° and 64.5° correspond to peaks assigned to the substrate; while a low intensity Ti peak originated from the Ti adhesion layer in as-deposited TiAlCN can be detected at 38.4°. An increase in crystallinity can be observed through the increase of peak intensities.

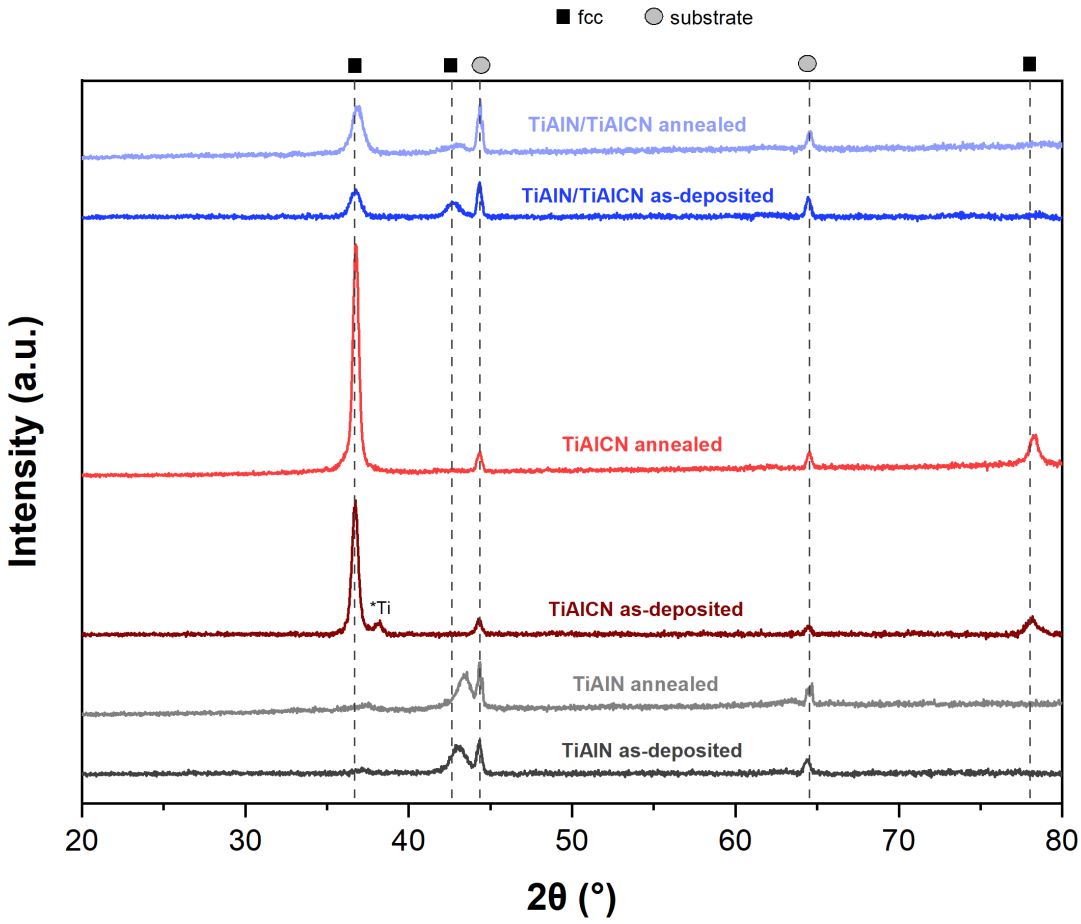

Figure 4.12 XRD diffractograms of as-deposited and annealed coatings.

4.6 Tribological Investigation

4.6.1 Coefficient of Friction

Figure 4.13, Figure 4.14 and Figure 4.15 show the evolution of the friction coefficient generated between the TiAlN, TiAlCN and TiAlN/TiAlCN coatings deposited on steel substrates against Al_2O_3 counterpart at room temperature, respectively. The coatings were subjected to 10 N and 5 N loads to mimic different types of loading applications. Furthermore, the number of cycles were set at 10000 and 20000 cycles to compare longevity of the coating wear resistance. All coatings except for the TiAlCN and TiAlN/TiAlCN tested under 5 N load for 10000 cycles exhibited two main stages in the friction coefficient curve: (1) running-in stage and (2) steady state stage. The running-in period indicates the cracking of the highest asperities on the coating and Al_2O_3 counterpart surfaces. The friction coefficient increases due to the entrapment of wear debris and oxides between the materials in contact, afterwards it reaches a stable value [41]. The other two coatings demonstrated a running-in stage, however, the friction coefficient value continued to increase until the end of the test; no steady state value has been achieved. The drastic perturbations present in the steady state region is attributed to the accumulation of both worn out coating and Al_2O_3 counterpart on the wear track during sliding. The presence of these debris is confirmed in the SEM micrograph of the wear track.

In general, the friction coefficient curves show that TiAlN coating displayed the highest COF while the multilayered TiAlN/TiAlCN coating displayed the lowest COF for all testing parameters. These results can be correlated to the hardness and toughness of the as-deposited coatings wherein TiAlN/TiAlCN displayed the highest H and E values while TiAlN coating exhibited the lowest values. The presence of C in the TiAlCN and TiAlN/TiAlCN is minimal for it to be a lubricating factor of the reduction in friction coefficient. As reported by Stueber et al. [50], C concentration must exceed 8 at.% for the soft amorphous phase to be present and act as a solid lubricant between the sliding components to reduce friction coefficient. The study of Tillmann et al. [16] is in good agreement with these results; the addition of C until 7.8 at.% in to the TiAlCN structure did not have noticeable impact to the COF values compared with TiAlN.

For the tribological test of as-deposited TiAlN coating using 10 N load for 10000 cycles, the running-in stage lasted for only a few cycles, then increasing steeply from the initial value of around 0.7 to approximately 0.9. On the other hand, the shift from the running-in stage to the steady stage states was not that drastic for 5 N load tested for 10000 and 20000 cycles. The running-in period lasted for about 2500 and 5000 cycles at a friction coefficient of 0.4. Afterwards, the friction curve suddenly increased to ~0.96 for tests at 10000 and 20000 cycles. As observed in Figure 4.13, the steady state stage for the friction curve of the 5 N load test has two apparent regions: (1) a higher friction coefficient value during the first few cycles of the steady state region and (2) drop to a lower friction until the end of the test. According to Tillman et al. [16], this behavior is related to the plastic deformation due to the smoothening of the two surfaces in contact, therefore reducing the ploughing factor in the friction coefficient.

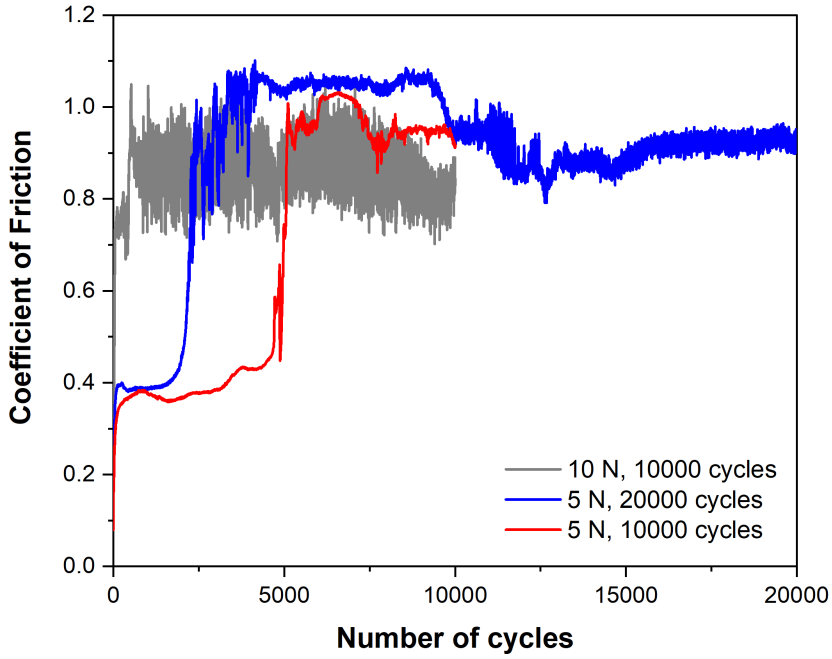

Figure 4.13 Friction coefficient curve of TiAlN tested against Al_2O_3 counterpart.

For as-deposited TiAlCN, a gradual increasing shift from running-in stage to steady state stage in the friction coefficient curves was observed for tests conducted at 10 N for 10000 cycles and 5 N for 20000 cycles, as shown in Figure 4.14. No steady state was observed for the coating tested at 5 N for 10000 cycles as the friction curve just increases from 0.2 to 0.6. The friction coefficient at the steady state stage is ~0.9 and ~0.7 for 10 N at 10000 cycles and 5 N for 20000 cycles, respectively.

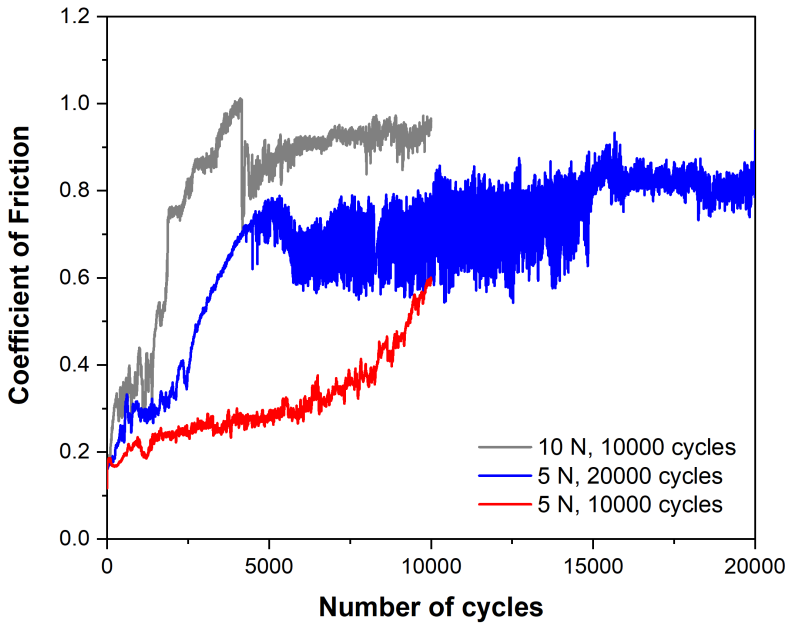

Figure 4.14 Friction coefficient curve of TiAlCN tested against Al_2O_3 counterpart.

For the as-deposited multilayered TiAlN/TiAlCN, an average of ~0.6 friction coefficient was observed for the coating tested at 10 N, as shown in Figure 4.15. A shorter running-in period towards a steady state value of ~0.7 was observed for the coating tested at 5 N for 20000 cycles, with several perturbations present. The sample tested at 5 N for 10000 cycles also displayed a long running-in stage and gradual increase of friction coefficient. No steady state stage was observed.

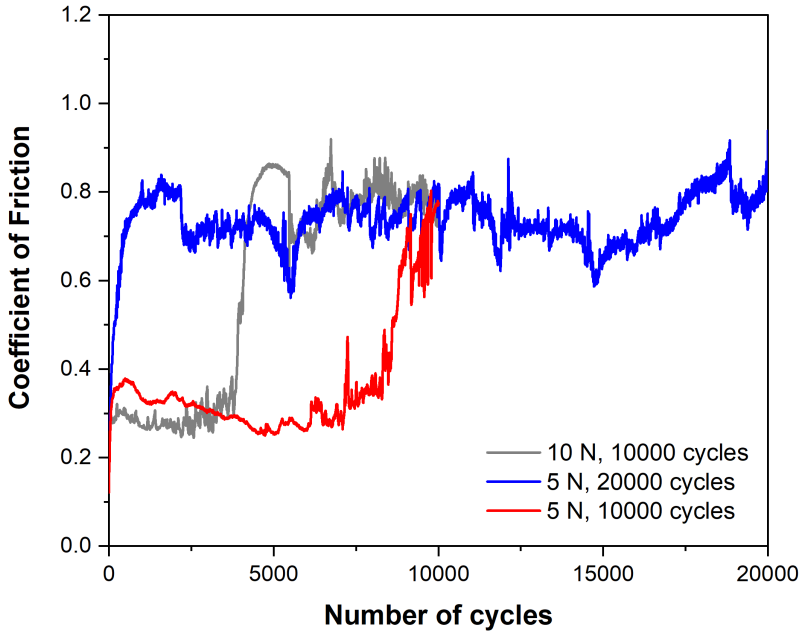

Figure 4.15 Friction coefficient curve of TiAlN/TiAlCN tested against Al_2O_3 counterpart.

4.6.2 Coating Wear Rate

Figure 4.16 shows the depth of wear track on the different coatings obtained after the tribological tests against Al_2O_3 counterpart. The wear track variation in the different coatings is in agreement with the behavior of the COF curves. The multilayered TiAlN/TiAlCN coating exhibited the shallowest wear track of ~0.2 μm at 5 N for 10000 cycles testing conditions. Globally, the multilayered coating exhibited the minimal depth of wear in all testing parameters which can be attributed to its high hardness and toughness compared with the monolithic TiAlN and TiAlCN coatings. The deepest wear track at ~5.5 μm was obtained for TiAlN coating subjected to 5 N for 20000 cycles. The wear depth exceeded the coating thickness signifying coating delamination which can explain the high friction coefficient value during sliding. Furthermore, the irregular surface profile can confirm the presence of wear debris along the sides and on the middle of the wear track. The coating delamination and presence of wear debris are confirmed by the SEM micrograph and EDS analysis of the wear tracks.

The coating wear rates calculated from the analysis of the wear depth for each test parameter are shown in Figure 4.17. As observed in Figure 4.13, 4.14 and 4.15, the coefficient of friction values of the coatings did not vary noticeably. However, there is significant difference of the tribological performance in terms of wear coefficients. In general, the wear rate and the friction coefficient value of the coatings exhibit a direct relationship between friction and wear. Under the same normal load and sliding conditions, monolithic TiAlN exhibited the highest COF and wear rate values while the multilayered TiAlN/TiAlCN reported the lowest COF and wear rate. The multilayered coating displayed the best wear rate performance for all parameters, which was expected due to the combination of its higher hardness, higher fracture toughness and lower friction coefficient compared with the monolithic coatings.

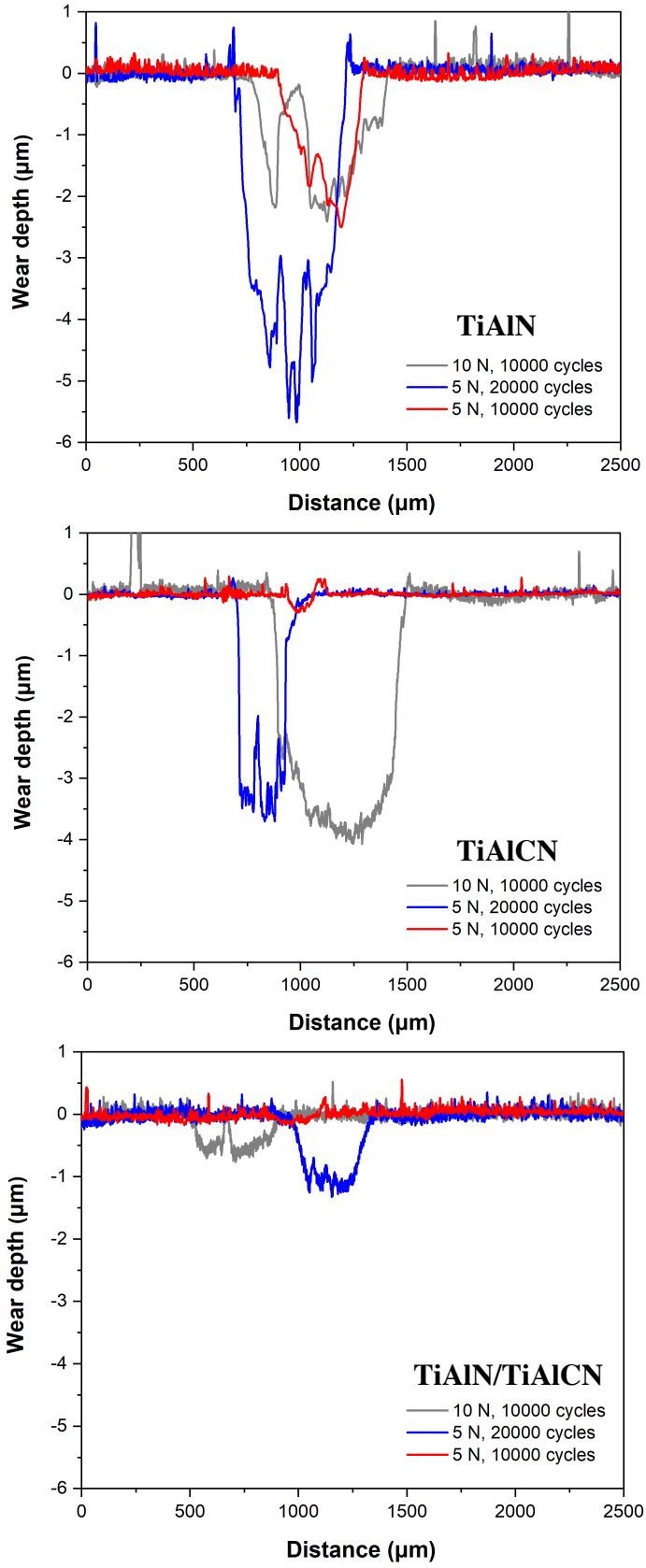

Figure 4.16 Depth of wear track for TiAlN, TiAlN and TiAlN/TiAlCN coatings tested against Al_2O_3 counterpart.

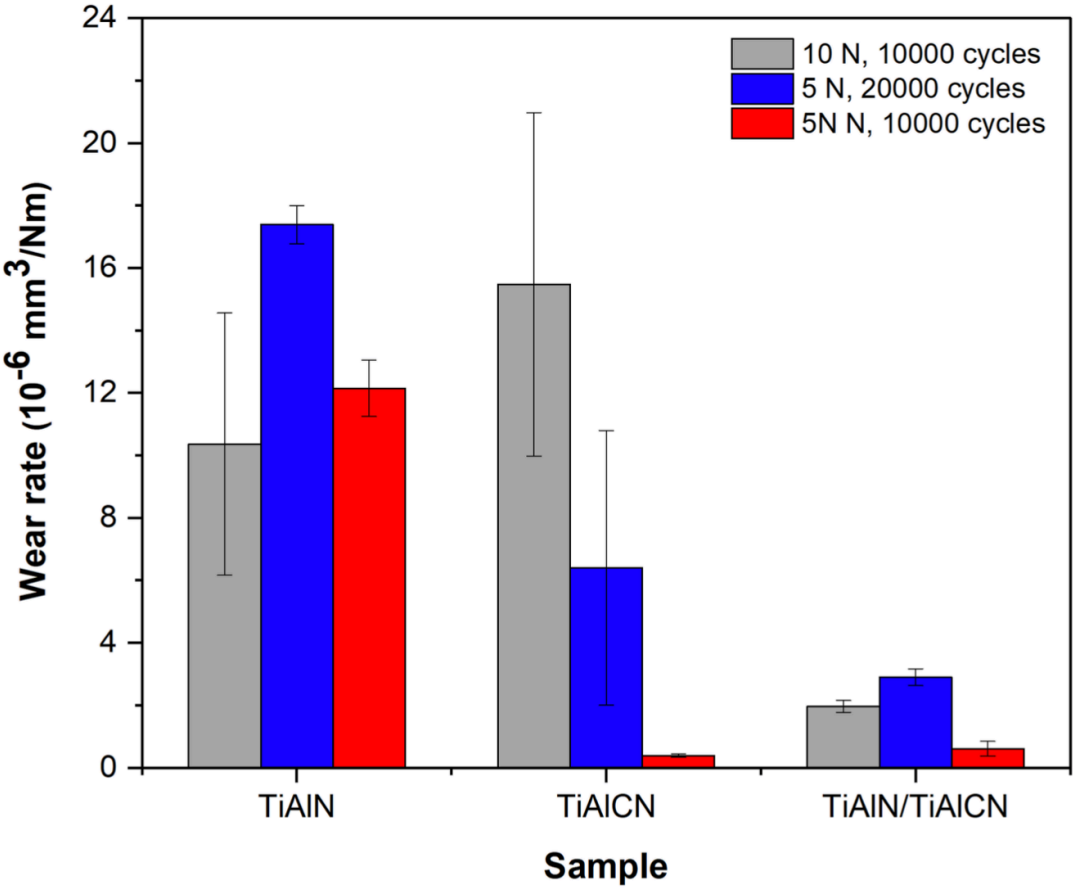

Figure 4.17 Specific wear rate of the coatings tested against Al_2O_3 counterpart.

Figure 4.18 displays the wear scar of counterpart alumina balls after the tribotest observed using an optical microscope. The images show grooves and the accumulation of wear debris on the wear scars which is largest on the counterpart used against TiAlN. These could be due to abrasive wear from the particles between the coating and the counterpart. Typically, the test condition where higher COF was measured resulted in larger wear scar of the alumina ball. The same results were observed in the study of Beliardouh et al. [60].

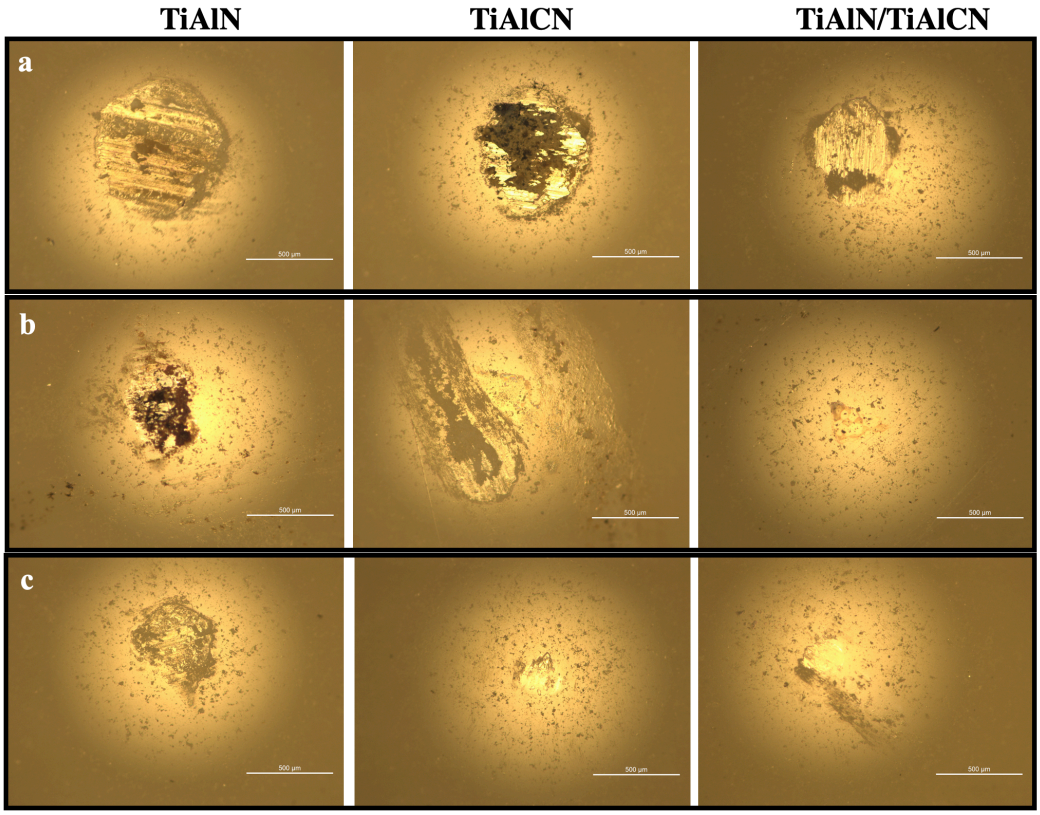

Figure 4.18 Wear track on Al_2O_3 balls for coatings tested at: (a) 10 N for 10000 cycles, (b) 5 N for 20000 cycles, and (c) 5 N for 10000 cycles.

4.6.3 Coating wear track

To understand the effect of COF and specific wear rate on the coating, the wear mechanism on the wear track were analyzed by SEM-EDS. Figures 4.19, 4.20 and 4.21 exhibit the results of wear mechanism analyses for TiAlN, TiAlCN and TiAlN/TiAlCN coatings, respectively. In general, the wear track seem to exhibit abrasion mechanism which is characterized by grooves and scratches and the presence of debris. Figures 4.19a and 4.19c show relatively smooth wear tracks with shallow grooves and ploughing wear scars parallel to the sliding direction for TiAlN. The EDS spectra of the debris revealed O and Al peaks and no substrate peaks, which can confirm presence of Al_2O_3 counterpart. Figure 4.19b shows delamination after 20000 cycles at 5 N load which is confirmed by the substrate peaks in the EDS. The continuous sliding movement of Al_2O_3 for a higher number of cycles along the coating surface contributed to the removal of the coating. The worn surface exhibits severe abrasive wear, in comparison with those tested at 10000 cycles. This also corroborates the measured depth of the wear track which exceeded the thickness of as-deposited coating.

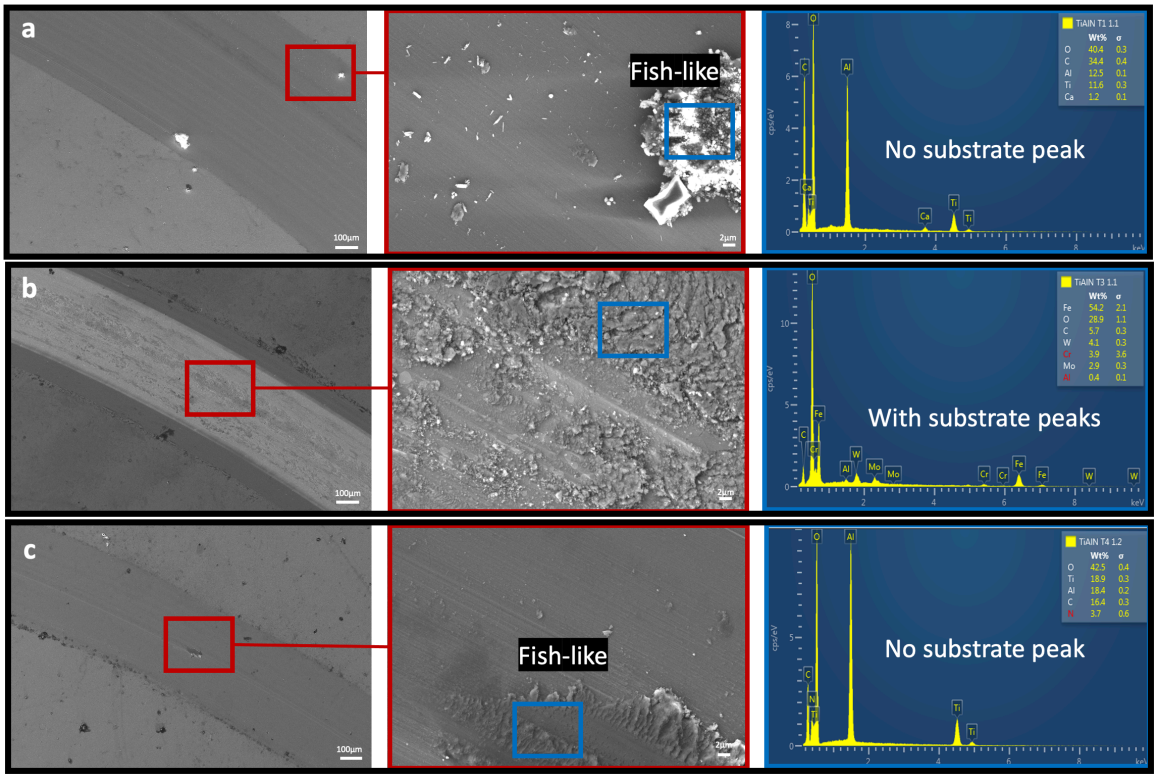

Figure 4.19 SEM of the wear tracks and EDS spectrum of the wear debris for TiAlN tested at: (a) 10 N for 10000 cycles, (b) 5 N for 20000 cycles and (c) 5 N for 10000 cycles.

The wear track of TiAlCN tested under 10 N for 10000 cycles shown in Figure 4.20a depicts abrasion mechanism. A region of the coating is delaminated as confirmed by the strong substrate peak in the EDS spectrum. This delaminated region is in the middle of the wear track where the highest cyclic contact stress stimulates propagation of through-thickness cracks [61]. Figure 4.20b also shows the presence of fish-like debris which is mostly composed of Al and O suggesting that the material must be from the Al_2O_3 counterpart with the Al at.% exceeding the as-deposited coating concentration. Minimal substrate peak may be from other regions on the coating with nominal coating delamination. In Figure 4.20c, no wear debris and coating delamination were observed, as confirmed by the EDS analysis. This test parameter also exhibited the shallowest wear depth and lowest COF value for TiAlCN coating.

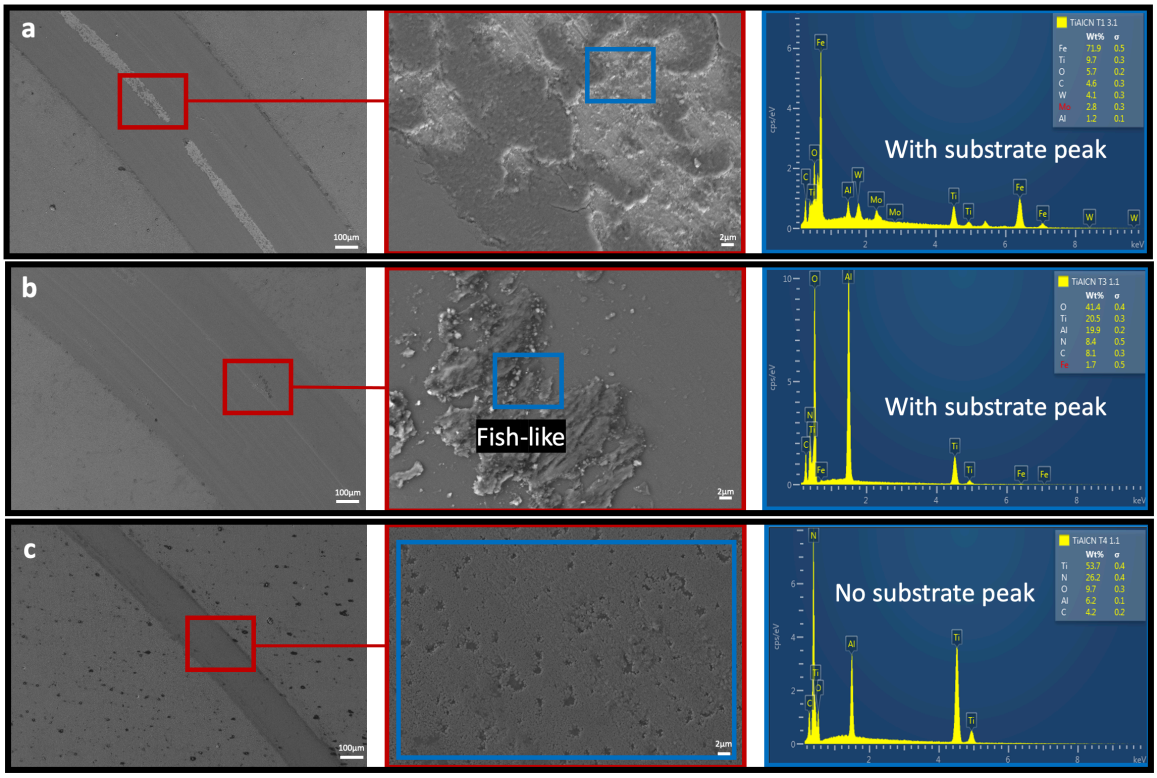

Figure 4.20 SEM of the wear tracks and EDS spectrum of the wear debris for TiAlCN tested at: (a) 10 N for 10000 cycles, (b) 5 N for 20000 cycles and (c) 5 N for 10000 cycles.

The wear track of TiAlN/TiAlCN tested under 10 N load for 10000 cycles shown in Figure 4.21a exhibits the formation of fish-like debris with strong O at.% based on EDS results. Due to the distinct grooves parallel to the direction of sliding, the wear was also governed by polishing mechanism with no apparent delamination. The multilayered coating which reported the lowest wear rate, exhibited a smooth wear track after being subjected to 5 N load for 10000 cycles, as shown in Figure 14.21c. The higher hardness and resistance to plastic deformation resulted in lower wear compared with the monolithic coatings. Scratches and ploughed regions can be observed on the surface wear track, but no coating delamination can be seen. At 5 N load tested for 20000 cycles, small regions of delamination can be observed. However, globally, the coating still exhibited smooth wear track. These findings corroborate the wear track depth measurement using the 2D profilometer. Wu et al. [62] investigated the tribological performance of TiAlCN deposited on WC-6%Co substrate against Si_3N_4 counterpart material and reported the same mechanical abrasion mechanism.

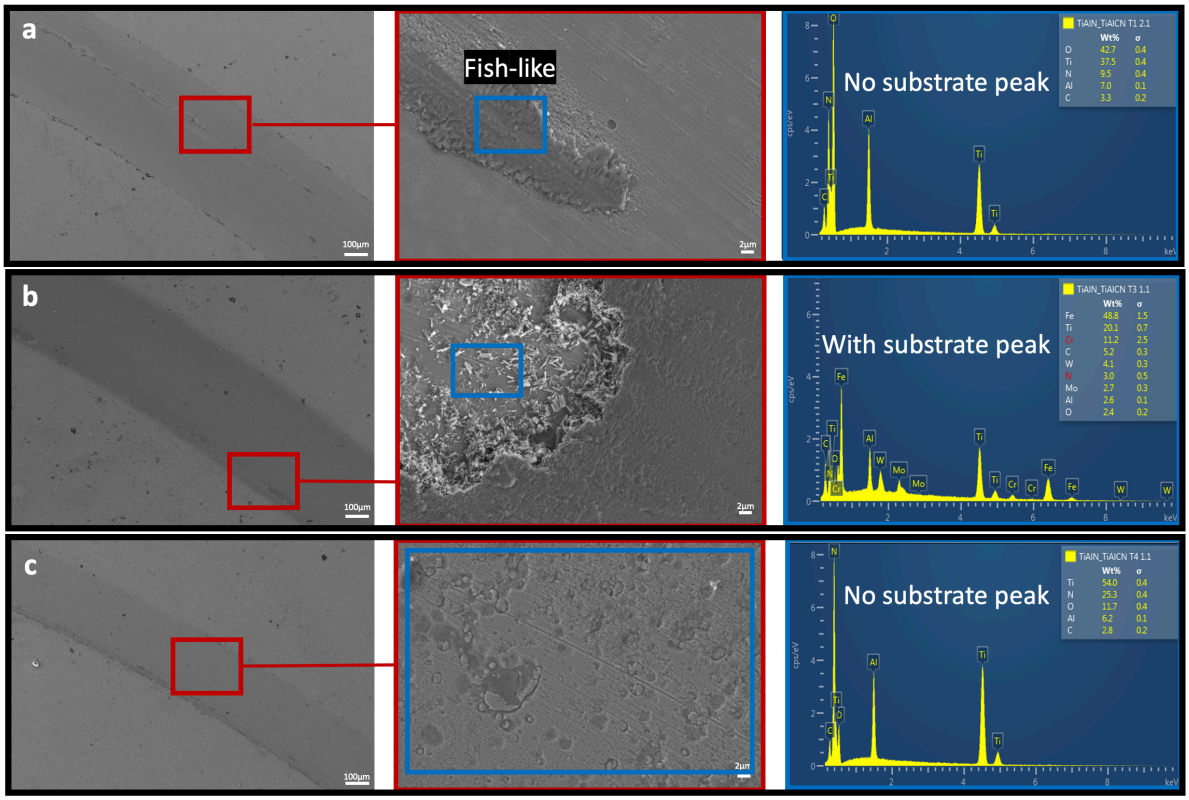

Figure 4.21 SEM of the wear tracks and EDS spectrum of the wear debris for TiAlN/TiAlCN tested at: (a) 10 N for 10000 cycles, (b) 5 N for 20000 cycles and (c) 5 N for 10000 cycles

It has been established in different studies that the H^3/E^2 ratio of plastic deformation are used to characterize the wear tribological properties of coatings [15,45,63]. High ratio value describes remarkable resistance to plastic deformation which means an improved ability to absorb energy during deformation until failure [41]. Thus, larger load is required to cause fracture or cracks, thereby increasing the resistance to wear of the coating [63]. Figure 4.22 shows a comparison between the H^3/E^2 ratio of the as-deposited coatings. The multilayered TiAlN/TiAlCN reported the highest value at 0.4. The result is corroborated with the higher wear resistance of the multilayered coating compared with the monolithic coatings at 0.2 and 0.25 for TiAlCN and TiAlN, respectively. The high hardness is beneficial in terms of increased resistance to plastic deformation. The multilayered TiAlN/TiAlCN presented the best tribological performance, delivering lower friction coefficient, high H^3/E^2 ratio and high hardness.

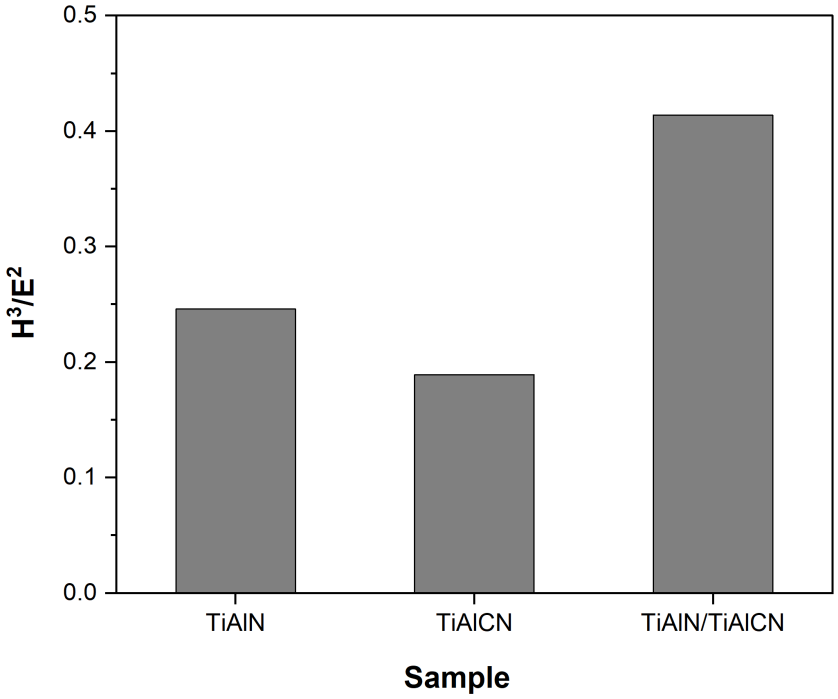

Figure 4.22 H^3/E^2 values of the as-deposited coatings.

CHAPTER 5: CONCLUSION

In this thesis, the morphology, structure, mechanical properties, thermal stability, oxidation resistance and tribological performance of industrial coatings, namely monolithic TiAlN and TiAlCN, and multilayered TiAlN/TiAlCN were investigated. The deposition was performed at an industrial coating enterprise via DC magnetron sputtering technique. The industrial coatings were developed using several cathode targets and different deposition parameters on various substrates.

The chemical analysis reported a 30.7 at.% Al content for TiAlN whilst TiAlCN and TiAlN/TiAlCN reported low value at 7.5 at.% and 8.1 at.%, respectively. Carbon was found to be within 5.5 – 6.6. at.%. All coatings exhibited a face centered cubic NaCl type structure with a (111) preferred orientation for TiAlN and (200) preferred orientation for TiAlCN and TiAlN/TiAlCN. The cross-section micrograph showed a columnar cross-section structure and typical cauliflower-like surface morphology. The multilayered TiAlN/TiAlCN displayed the best adhesion strength onto the steel substrate. All coatings did not show any sign of delamination at 70 N critical load. The high Al improved the oxidation resistance of TiAlN to be at ~900°C while TiAlCN and TiAlN/TiAlCN demonstrated oxidation resistance until ~850°C and ~800°C, respectively. The improved oxidation resistance of TiAlN-based coatings is due to the formation of a thermally stable oxide scale comprised of dense Al_2O_3 upper layer. By the end of the isothermal oxidation test at 900°C for 2 h, the coatings were fully oxidized except for TiAlN. The XRD and SEM-EDS analyses of oxidized coatings confirmed the formation of the oxide scale on the surface. The as-deposited multilayered TiAlN/TiAlCN exhibited the highest hardness as the interfaces present in the multilayered structure hindered movement of dislocations and allowed distribution of stress among the single components. On the other hand, TiAlN demonstrated the highest hardness upon annealing at 800°C for 2 h which can be attributed to increase in crystallinity. The crystal structure remained relatively stable for all coatings after annealing which demonstrates the superior thermal stability of TiAlN-based coatings.

The present work also investigated the room temperature tribological performance of coatings deposited on steel against Al_2O_3 counterpart. The parameters were varied according to load and cycle number. The wear mechanism and wear debris were characterized by SEM

and EDS and were correlated with the friction coefficient and wear rate values of the coating. Generally, the friction curves reported two stages: (1) running-in stage and (2) steady stage. The wear depth and track corroborate the friction coefficient and hardness variation results. The wear tracks seem to exhibit abrasion mechanism which is characterized by grooves and scratches and the presence of wear debris in fish-like form. The EDS analysis confirmed the presence of substrate for wear track depth that exceeded coating thickness. The multilayered TiAlN/TiAlCN coating presented the best tribological performance due to the combination of low friction coefficient, high hardness, and high H^3/E^2 ratio.

CHAPTER 6: FUTURE WORK

The following recommendations are proposed for future studies related to this work:

i. Evaluate the tribological performance of the industrial coatings using pin-on-disk test at higher operating temperature ranging from 500°C to 800°C
ii. Evaluate the machining performance of the industrial coatings under different drilling conditions against Ti6Al4V alloy workpiece
iii. Investigate the tribological performance of annealed industrial coatings
iv. Deposit industrial coatings with higher C content to assess the solid lubrication mechanism of amorphous C during tribological test

REFERENCES

[1] Ezugwu, E., Bonney, J., & Yamane, Y. (2003). An overview of the machinability of aeroengine alloys. *Journal of Materials Processing Technology*, *134*(2), 233–253. https://doi.org/10.1016/s0924-0136(02)01042-7

[2] Shokrani, A., Dhokia, V., & Newman, S. (2012). Environmentally conscious machining of difficult-to-machine materials with regard to cutting fluids. *International Journal of Machine Tools and Manufacture*, *57*, 83–101. https://doi.org/10.1016/j.ijmachtools.2012.02.002

[3] Singh, P., Pungotra, H., & Kalsi, N. S. (2017). On the characteristics of titanium alloys for the aircraft applications. *Materials Today: Proceedings*, *4*(8), 8971–8982. https://doi.org/10.1016/j.matpr.2017.07.249

[4] Pramanik, A. (2013). Problems and solutions in machining of titanium alloys. *The International Journal of Advanced Manufacturing Technology*, *70*(5–8), 919–928. https://doi.org/10.1007/s00170-013-5326-x

[5] Cui, C., Hu, B., Zhao, L., & Liu, S. (2011). Titanium alloy production technology, market prospects and industry development. *Materials & Design*, *32*(3), 1684–1691. https://doi.org/10.1016/j.matdes.2010.09.011

[6] Froes, F. H. (Ed.). (2016). Applications of Titanium [E-book]. In *Titanium: physical metallurgy, processing, and applications* (1st ed., pp. 353–380). ASM International.

[7] Campbell, F. C. (Ed.). (2013). Machining. In *Metals Fabrication: Understanding the Basics* (pp. 213–270). ASM International.

[8] Yang, X., & Richard Liu, C. (1999). Machining titanium and its alloys. *Machining Science and Technology*, *3*(1), 107–139. https://doi.org/10.1080/10940349908945686

[9] Pramanik, A., & Littlefair, G. (2015). Machining of Titanium Alloy (Ti-6Al-4V)—Theory to Application. *Machining Science and Technology*, *19*(1), 1–49. https://doi.org/10.1080/10910344.2014.991031

[10] Sousa, V. F. C., da Silva, F. J. G., Pinto, G. F., Baptista, A., & Alexandre, R. (2021). Characteristics and Wear Mechanisms of TiAlN-Based Coatings for Machining Applications: A Comprehensive Review. *Metals*, *11*(2), 260. https://doi.org/10.3390/met11020260

[11] Singh, G., Aggarwal, V., & Singh, S. (2020). Critical review on ecological, economical and technological aspects of minimum quantity lubrication towards sustainable machining. *Journal of Cleaner Production*, *271*, 122185. https://doi.org/10.1016/j.jclepro.2020.122185

[12] Revuru, R. S., Posinasetti, N. R., VSN, V. R., & M, A. (2017). Application of cutting fluids in machining of titanium alloys—a review. *The International Journal of Advanced Manufacturing Technology*, *91*(5–8), 2477–2498. https://doi.org/10.1007/s00170-016-9883-7

[13] PalDey, S., & Deevi, S. (2003). Single layer and multilayer wear resistant coatings of (Ti,Al)N: a review. *Materials Science and Engineering: A*, *342*(1–2), 58–79. https://doi.org/10.1016/s0921-5093(02)00259-9

[14] Geng, Z., Shi, G., Shao, T., Liu, Y., Duan, D., & Reddyhoff, T. (2019). Tribological behavior of patterned TiAlN coatings at elevated temperatures. *Surface and Coatings Technology*, *364*, 99–114. https://doi.org/10.1016/j.surfcoat.2019.02.076

[15] Rashidi, M., Tamizifar, M., & Ali Boutorabi, S. M. (2020). Characteristics of TiAlCN ceramic coatings prepared via pulsed-DC PACVD, part I: Influence of precursors' ratio. *Ceramics International*, *46*(2), 1269–1280. https://doi.org/10.1016/j.ceramint.2019.06.303

[16] Tillmann, W., Grisales, D., Marin Tovar, C., Contreras, E., Apel, D., Nienhaus, A., Stangier, D., & Lopes Dias, N. F. (2020). Tribological behaviour of low carbon-containing TiAlCN coatings deposited by hybrid (DCMS/HiPIMS) technique. *Tribology International*, *151*, 106528. https://doi.org/10.1016/j.triboint.2020.106528

[17] Zhang, M., Cheng, Y., Xin, L., Su, J., Li, Y., Zhu, S., & Wang, F. (2020). Cyclic oxidation behaviour of Ti/TiAlN composite multilayer coatings deposited on titanium alloy. *Corrosion Science*, *166*, 108476. https://doi.org/10.1016/j.corsci.2020.108476

[18] Sahul, M., Haršáni, M., Babincová, P., ČAplovič, L., Sahul, M., & Drobný, P. (2020). Deposition and characterization of Ti-Al-C-N coatings. IOP Conference Series: *Materials Science and Engineering*, *726*, 012013. https://doi.org/10.1088/1757-899x/726/1/012013

[19] Goindi, G. S., & Sarkar, P. (2017). Dry machining: A step towards sustainable machining – Challenges and future directions. *Journal of Cleaner Production*, *165*, 1557–1571. https://doi.org/10.1016/j.jclepro.2017.07.235

[20] Gao, Y., Wang, G., & Liu, B. (2016). Chip formation characteristics in the machining of titanium alloys: a review. *International Journal of Machining and Machinability of Materials*, *18*(1/2), 155. https://doi.org/10.1504/ijmmm.2016.075467

[21] Rizzo, A., Goel, S., Luisa Grilli, M., Iglesias, R., Jaworska, L., Lapkovskis, V., Novak, P., Postolnyi, B. O., & Valerini, D. (2020). The Critical Raw Materials in Cutting Tools for Machining Applications: A Review. *Materials*, *13*(6), 1377. https://doi.org/10.3390/ma13061377

[22] Ezugwu, E. O., & Wang, Z. M. (1997). Titanium alloys and their machinability—a review. *Journal of Materials Processing Technology*, *68*(3), 262–274. https://doi.org/10.1016/S0924-0136(96)00030-1

[23] Trent, E. M. (2000). Cutting Tool Materials II: Cemented Carbides. In P. K. Wright (Ed.), *Metal Cutting* (4th ed., pp. 175–226). Butterworth-Heinemann. https://doi.org/10.1016/B978-0-7506-7069-2.X5000-1

[24] Sharma, V. S., Dogra, M., & Suri, N. (2009). Cooling techniques for improved productivity in turning. *International Journal of Machine Tools and Manufacture*, *49*(6), 435–453. https://doi.org/10.1016/j.ijmachtools.2008.12.010

[25] Abdalla, H. S., Baines, W., McIntyre, G., & Slade, C. (2006). Development of novel sustainable neat-oil metal working fluids for stainless steel and titanium alloy machining. Part 1. Formulation development. *The International Journal of Advanced Manufacturing Technology*, *34*(1–2), 21–33. https://doi.org/10.1007/s00170-006-0585-4

[26] Chetan, Ghosh, S., & Venkateswara Rao, P. (2015). Application of sustainable techniques in metal cutting for enhanced machinability: a review. *Journal of Cleaner Production*, *100*, 17–34. https://doi.org/10.1016/j.jclepro.2015.03.039

[27] ŁęPicka, M., Grądzka-Dahlke, M., Pieniak, D., Pasierbiewicz, K., Kryńska, K., & Niewczas, A. (2019). Tribological performance of titanium nitride coatings: A comparative study on TiN-coated stainless steel and titanium alloy. *Wear*, *422–423*, 68–80. https://doi.org/10.1016/j.wear.2019.01.029

[28] Peng, Z., Miao, H., Qi, L., Yang, S., & Liu, C. (2003). Hard and wear-resistant titanium nitride coatings for cemented carbide cutting tools by pulsed high energy density plasma. *Acta Materialia*, *51*(11), 3085–3094. https://doi.org/10.1016/s1359-6454(03)00119-8

[29] Kelly, P., vom Braucke, T., Liu, Z., Arnell, R., & Doyle, E. (2007). Pulsed DC titanium nitride coatings for improved tribological performance and tool life. *Surface and Coatings Technology*, *202*(4–7), 774–780. https://doi.org/10.1016/j.surfcoat.2007.07.047

[30] Zhang, X., Qiu, Y., Tan, Z., Lin, J., Xu, A., Zeng, Y., Moore, J., & Jiang, J. (2014). Effect of Al content on structure and properties of TiAlCN coatings prepared by magnetron sputtering. *Journal of Alloys and Compounds*, *617*, 81–85. https://doi.org/10.1016/j.jallcom.2014.08.009

[31] Qi, Z., Sun, P., Zhu, F., Wu, Z., Liu, B., Wang, Z., Peng, D., & Wu, C. (2013). Relationship between tribological properties and oxidation behavior of $Ti_{0.34}Al_{0.66}N$ coatings at elevated temperature up to 900°C. *Surface and Coatings Technology*, *231*, 267–272. https://doi.org/10.1016/j.surfcoat.2012.02.017

[32] Zhou, M., Makino, Y., Nose, M., & Nogi, K. (1999). Phase transition and properties of Ti–Al–N thin films prepared by r.f.-plasma assisted magnetron sputtering. *Thin Solid Films*, *339*(1–2), 203–208. https://doi.org/10.1016/s0040-6090(98)01364-9

[33] Chang, C. L., & Yang, F. C. (2019). Reprint of "Effect of target composition on the microstructural, mechanical, and corrosion properties of TiAlN thin films deposited by high-power impulse magnetron sputtering." *Surface and Coatings Technology*, *376*, 124784. https://doi.org/10.1016/j.surfcoat.2019.07.008

[34] Yoon, S. Y., Lee, K. O., Kang, S. S., & Kim, K. H. (2002). Comparison for mechanical properties between TiN and TiAlN coating layers by AIP technique. *Journal of Materials Processing Technology*, *130–131*, 260–265. https://doi.org/10.1016/s0924-0136(02)00746-x

[35] Polcar, T., Novák, R., & ŠIroký, P. (2006). The tribological characteristics of TiCN coating at elevated temperatures. *Wear*, *260*(1–2), 40–49. https://doi.org/10.1016/j.wear.2004.12.031

[36] Hernández-Sierra, M. T., Aguilera-Camacho, L. D., Ponce, A., García-Miranda, J. S., & Moreno, K. J. (2018). Tribological performance of TiN and TiCN coatings on a working tool steel. *Journal of Mechanical Science and Technology*, *32*(8), 3659–3666. https://doi.org/10.1007/s12206-018-0718-3

[37] Lei, Z., Zhu, X., Li, Y., Song, Z., Liu, H., & Fu, Y. Q. (2018). Characterization and Tribological Behavior of TiAlN/TiAlCN Multilayer Coatings. *Journal of Tribology*, *140*(5). https://doi.org/10.1115/1.4039723

[38] Zhang, X., Jiang, J., Yuqiao, Z., Lin, J., Wang, F., & Moore, J. J. (2008). Effect of carbon on TiAlCN coatings deposited by reactive magnetron sputtering. *Surface and Coatings Technology*, *203*(5–7), 594–597. https://doi.org/10.1016/j.surfcoat.2008.06.175

[39] Zeng, Y., Qiu, Y., Mao, X., Tan, S., Tan, Z., Zhang, X., Chen, J., & Jiang, J. (2015). Superhard TiAlCN coatings prepared by radio frequency magnetron sputtering. *Thin Solid Films*, *584*, 283–288. https://doi.org/10.1016/j.tsf.2015.02.068

[40] Vereschaka, A., Grigoriev, S., Vereschaka, A., Popov, A., & Batako, A. (2014). Nano-scale Multilayered Composite Coatings for Cutting Tools Operating under Heavy Cutting Conditions. *Procedia CIRP*, *14*, 239–244. https://doi.org/10.1016/j.procir.2014.03.070

[41] AL-Bukhaiti, M., Al-hatab, K., Tillmann, W., Hoffmann, F., & Sprute, T. (2014). Tribological and mechanical properties of Ti/TiAlN/TiAlCN nanoscale multilayer PVD coatings deposited on AISI H11 hot work tool steel. *Applied Surface Science*, *318*, 180–190. https://doi.org/10.1016/j.apsusc.2014.03.026

[42] Rizzo, A., Mirenghi, L., Massaro, M., Galietti, U., Capodieci, L., Terzi, R., Tapfer, L., & Valerini, D. (2013). Improved properties of TiAlN coatings through the multilayer structure. *Surface and Coatings Technology*, *235*, 475–483. https://doi.org/10.1016/j.surfcoat.2013.08.006

[43] Kawata, K., Sugimura, H., & Takai, O. (2001). Characterization of multilayer films of Ti-Al-O-C-N system prepared by pulsed d.c. plasma-enhanced chemical vapor deposition. *Thin Solid Films*, *390*(1–2), 64–69. https://doi.org/10.1016/s0040-6090(01)00939-7

[44] Chen, S., Zhao, Y., Zhang, Y., Chen, L., Liao, B., Zhang, X., & Ouyang, X. (2021). Influence of carbon content on the structure and tribocorrosion properties of TiAlCN/TiAlN/TiAl multilayer composite coatings. *Surface and Coatings Technology*, *411*, 126886. https://doi.org/10.1016/j.surfcoat.2021.126886

[45] Jindal, P., Santhanam, A., Schleinkofer, U., & Shuster, A. (1999). Performance of PVD TiN, TiCN, and TiAlN coated cemented carbide tools in turning. *International Journal of Refractory Metals and Hard Materials*, *17*(1–3), 163–170. https://doi.org/10.1016/s0263-4368(99)00008-6

[46] Sharif, S., & Rahim, E. (2007). Performance of coated- and uncoated-carbide tools when drilling titanium alloy—Ti–6Al4V. *Journal of Materials Processing Technology*, *185*(1–3), 72–76. https://doi.org/10.1016/j.jmatprotec.2006.03.142

[47] Vereschaka, A. A., Grigoriev, S. N., Sitnikov, N. N., Oganyan, G. V., & Batako, A. (2017). Working efficiency of cutting tools with multilayer nano-structured Ti-TiCN-(Ti,Al)CN and Ti-TiCN-(Ti,Al,Cr)CN coatings: Analysis of cutting properties, wear mechanism and diffusion processes. *Surface and Coatings Technology*, *332*, 198–213. https://doi.org/10.1016/j.surfcoat.2017.10.027

[48] Jacobs, R., Meneve, J., Dyson, G., Teer, D., Jennett, N., Harris, P., von Stebut, J., Comte, C., Feuchter, P., Cavaleiro, A., Ronkainen, H., Holmberg, K., Beck, U., Reiners, G., & Ingelbrecht, C. (2003). A certified reference material for the scratch test. *Surface and Coatings Technology*, *174–175*, 1008–1013. https://doi.org/10.1016/s0257-8972(03)00470-5

[49] Archard, J. F. (1953). Contact and Rubbing of Flat Surfaces. *Journal of Applied Physics*, *24*(8), 981–988. https://doi.org/10.1063/1.1721448

[50] Stueber, M., Barna, P., Simmonds, M., Albers, U., Leiste, H., Ziebert, C., Holleck, H., Kovács, A., Hovsepian, P., & Gee, I. (2005). Constitution and microstructure of magnetron sputtered nanocomposite coatings in the system Ti–Al–N–C. *Thin Solid Films*, *493*(1–2), 104–112. https://doi.org/10.1016/j.tsf.2005.07.290

[51] Jang, C. S., Jeon, J. H., Song, P. K., Kang, M. C., & Kim, K. H. (2005). Synthesis and mechanical properties of $TiAlC_xN_{1-x}$ coatings deposited by arc ion plating. *Surface and Coatings Technology*, *200*(5–6), 1501–1506. https://doi.org/10.1016/j.surfcoat.2005.08.065

[52] Shugurov, A. R., & Kazachenok, M. S. (2018). Mechanical properties and tribological behavior of magnetron sputtered TiAlN/TiAl multilayer coatings. *Surface and Coatings Technology*, *353*, 254–262. https://doi.org/10.1016/j.surfcoat.2018.09.001

[53] Panjan, P., Drnovšek, A., & Dražić, G. (2021). *Influence of Growth Defects on the Oxidation Resistance of Sputter-Deposited TiAlN Hard Coatings*. *Coatings*, *11*(2), 123. https://doi.org/10.3390/coatings11020123

[54] Peng, J., Su, D., & Wang, C. (2014). Combined Effect of Aluminum Content and Layer Structure on the Oxidation Performance of $Ti_{1-x}Al_xN$ Based Coatings. *Journal of Materials Science & Technology*, *30*(8), 803–807. https://doi.org/10.1016/j.jmst.2014.03.020

[55] Kamath, G., Ehiasarian, A., Purandare, Y., & Hovsepian, P. (2011). Tribological and oxidation behaviour of TiAlCN/VCN nanoscale multilayer coating deposited by the

combined HIPIMS/(HIPIMS-UBM) technique. *Surface and Coatings Technology*, *205*(8–9), 2823–2829. https://doi.org/10.1016/j.surfcoat.2010.10.049

[56] Zhou, J., Hu, C., Zhang, J., Chen, L., & Kong, Y. (2021). Effect of B-doping on the mechanical properties, thermal stability and oxidation resistance of TiAlN coatings. *International Journal of Refractory Metals and Hard Materials*, *98*, 105531. https://doi.org/10.1016/j.ijrmhm.2021.105531

[57] Colombo, D. A., Mandri, A. D., Echeverría, M. D., Massone, J. M., & Dommarco, R. C. (2018). Mechanical and tribological behavior of Ti/TiN and TiAl/TiAlN coated austempered ductile iron. *Thin Solid Films*, *647*, 19–25. https://doi.org/10.1016/j.tsf.2017.12.014

[58] Bartosik, M., Rumeau, C., Hahn, R., Zhang, Z. L., & Mayrhofer, P. H. (2017). Fracture toughness and structural evolution in the TiAlN system upon annealing. Scientific Reports, 7(1). https://doi.org/10.1038/s41598-017-16751-1

[59] Shtansky, D., Kiryukhantsev-Korneev, P., Sheveyko, A., Mavrin, B., Rojas, C., Fernandez, A., & Levashov, E. (2009). Comparative investigation of TiAlC(N), TiCrAlC(N), and CrAlC(N) coatings deposited by sputtering of MAX-phase $Ti_{2-x}Cr_xAlC$ targets. *Surface and Coatings Technology*, *203*(23), 3595–3609. https://doi.org/10.1016/j.surfcoat.2009.05.036

[60] Beliardouh, N. E., Nouveau, C., Walock, M. J., & Jacquet, P. (2014). A study of the wear performance of duplex treated commercial low-alloy steel against alumina and WC balls. Surface and Coatings Technology, 259, 483–494. https://doi.org/10.1016/j.surfcoat.2014.10.042

[61] Rizzo, A., Mirenghi, L., Massaro, M., Galietti, U., Capodieci, L., Terzi, R., Tapfer, L., & Valerini, D. (2013). Improved properties of TiAlN coatings through the multilayer structure. *Surface and Coatings Technology*, *235*, 475–483. https://doi.org/10.1016/j.surfcoat.2013.08.006

[62] Wu, W., Liu, J., Hua, T., Chen, Z., Jiang, J., Wang, H., Liu, L., & Liu, X. (2018). Microstructure and Friction-Wear Behavior of Multi-arc Ion Plating TiAlNC Ceramic Coating on WC-6%Co Substrate. *Journal of Materials Engineering and Performance*, *27*(9), 4665–4671. https://doi.org/10.1007/s11665-018-3568-3

[63] Yang, Y., Shang, H., & Shao, T. (2020). Influence of nitrogen implantation on adhesion strength of TiAlN film on γ-TiAl alloy. *Applied Surface Science*, *508*, 145141. https://doi.org/10.1016/j.apsusc.2019.145141